JACC: BASIC TO TRANSLATIONAL SCIENCE VOL. ■, NO. ■, 2022

CLINICAL RESEARCH

Cardiac Transcriptome Remodeling and Impaired Bioenergetics in Single-Ventricle Congenital Heart Disease

Anastacia M. Garcia, PhD,[a] Lee S. Toni, PhD,[b] Carissa A. Miyano, MS,[b] Genevieve C. Sparagna, PhD,[b] Raleigh Jonscher, BS,[b] Elisabeth K. Phillips, MS,[b] Anis Karimpour-Fard, PhD,[c] Hailey L. Chapman, BS,[a] Angela N. Baybayon-Grandgeorge, BS,[b] Ashley E. Pietra, BS,[a] Emma Selner, BS,[a] Kathryn C. Chatfield, MD, PhD,[a] Brian L. Stauffer, MD,[b,d] Carmen C. Sucharov, PhD,[b] Shelley D. Miyamoto, MD[a]

VISUAL ABSTRACT

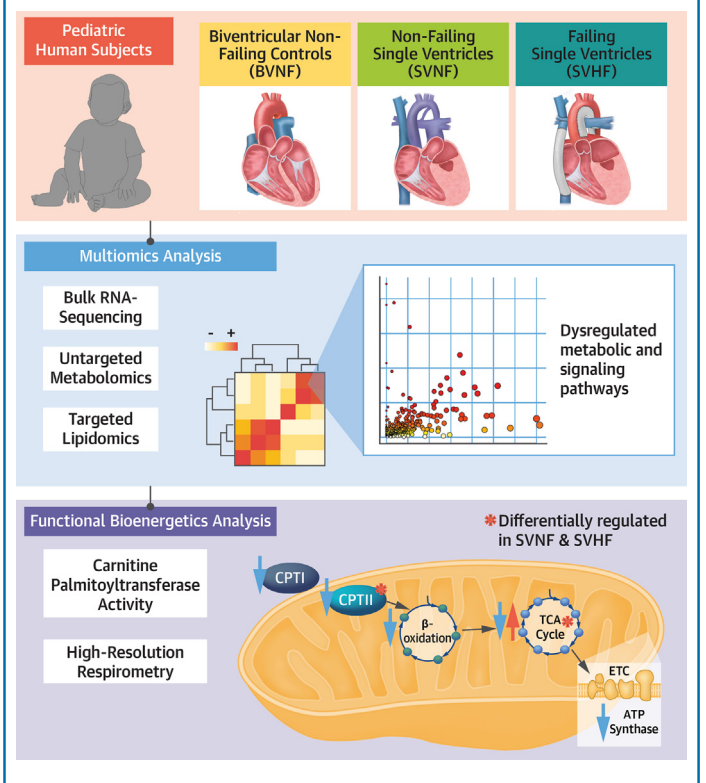

Garcia AM, et al. J Am Coll Cardiol Basic Trans Science. 2022;■(■):■–■.

HIGHLIGHTS

- **This study represents a comprehensive characterization of the transcriptome combined with functional mitochondrial studies in SV CHD myocardium.**
- **The *failing* SV heart shows alterations in metabolic gene expression and impaired energy generation with diminished ATP and phosphocreatine levels. Decreased activity of mitochondrial CPT transporters may account for abnormalities in OXPHOS leading to an inability of the failing SV to generate maximal respiratory capacity.**
- **The *nonfailing* SV heart demonstrates an intermediate metabolic phenotype suggesting that the SV heart is inherently vulnerable to eventual failure, thus providing some insights into the transition from health to disease in SV CHD.**

From the [a]Division of Cardiology, Department of Pediatrics, University of Colorado Anschutz Medical Campus, Children's Hospital Colorado, Aurora, Colorado, USA; [b]Division of Cardiology, Department of Medicine, University of Colorado Anschutz Medical Campus, Aurora, Colorado, USA; [c]Department of Pharmacology, University of Colorado Anschutz Medical Campus, Aurora, Colorado, USA; and the [d]Division of Cardiology, Department of Medicine, Denver Health and Hospital Authority, Denver, Colorado, USA.

The authors attest they are in compliance with human studies committees and animal welfare regulations of the authors' institutions and Food and Drug Administration guidelines, including patient consent where appropriate. For more information, visit the Author Center.

Manuscript received April 11, 2022; revised manuscript received September 28, 2022, accepted September 28, 2022.

ISSN 2452-302X https://doi.org/10.1016/j.jacbts.2022.09.013

ABBREVIATIONS AND ACRONYMS

AA = amino acid

ADP = adenosine diphosphate

ANOVA = analysis of variance

ATP = adenosine triphosphate

BCAA = branched-chain amino acid

BVNF = biventricular nonfailing

CHD = congenital heart disease

CoA = coenzyme A

CPT = carnitine palmitoyltransferase

DEG = differentially expressed gene

DEM = differentially expressed metabolite

FA = fatty acid

GO = Gene Ontology

HF = heart failure

HLHS = hypoplastic left heart syndrome

LC = liquid chromatography

LV = left ventricle

MS = mass spectrometry

β-OX = β-oxidation

OXPHOS = oxidative phosphorylation

PANTHER = Protein Analysis Through Evolutionary Relationships

PCA = principal component analysis

RNA-Seq = RNA sequencing

RV = right ventricle

SV = single ventricle

SVHF = single-ventricle heart failure

SVHFpEF = single-ventricle heart failure with preserved ejection fraction (systolic function)

SVHFrEF = single-ventricle heart failure with reduced ejection fraction (systolic function)

SVNF = single-ventricle nonfailing

TCA = tricarboxylic acid

UPLC = ultrahigh-pressure liquid chromatography

SUMMARY

The mechanisms responsible for heart failure in single-ventricle congenital heart disease are unknown. Using explanted heart tissue, we showed that failing single-ventricle hearts have dysregulated metabolic pathways, impaired mitochondrial function, decreased activity of carnitine palmitoyltransferase activity, and altered functioning of the tricarboxylic acid cycle. Interestingly, nonfailing single-ventricle hearts demonstrated an intermediate metabolic phenotype suggesting that they are vulnerable to development of heart failure in the future. Mitochondrial targeted therapies and treatments aimed at normalizing energy generation could represent a novel approach to the treatment or prevention of heart failure in this vulnerable group of patients. (J Am Coll Cardiol Basic Trans Science 2022;■:■–■)

Although 1% of children are born with congenital heart disease (CHD),[1] there are limited treatment options for those patients with the most complex CHDs, such as single-ventricle CHD (SV). SV is the most common complex CHD and represents a heterogeneous group of anatomical cardiac defects typified by severe underdevelopment of 1 side of the heart that results in a univentricular circulation. Patients with SV have a higher risk of mortality than patients with any other CHD. Patients with a systemic right ventricle (RV) in particular, such as those with hypoplastic left heart syndrome (HLHS), represent the most common SV subtype and tend to have worse outcomes.[2-11] Because the geometry, fiber orientation, and metabolic adaptations of the RV are not tailored to support the high-pressure systemic circulation, patients with SV of right ventricular morphology are at particularly increased risk of morbidity and mortality.[2-11] Given the poor outcomes in this subgroup, patients with SV of right ventricular morphology (including those with HLHS) are the focus of this study.

SV is universally fatal without surgical intervention or heart transplantation; however, in the past several decades, remarkable advances in surgical techniques and postoperative care have resulted in an increasing number of patients with SV living into adulthood. It is estimated that there are approximately 1.6 per 10,000 children and young adults living with SV physiology today.[12] Nevertheless, despite the growing numbers of child and adult survivors with SV, hypertrophy, remodeling, and eventual heart failure (HF) are important lifelong sequelae after palliative surgical repair in these patients.[13-16] Patients with SV therefore require a substantial investment of health care resources over their lifetime, and their long-term prognosis remains guarded even after surviving the early neonatal period.[17] Importantly, more than 30% of patients with SV die or require cardiac transplantation within the first year of life, and 10-year survival in these patients is only 39% to 50%.[8,18] In a normal heart, the RV supports the low-pressure pulmonary circulation; however, in patients with a single RV, the RV must adapt to sustain systemic perfusion. Therefore, long-term survival and quality of life ultimately depend on preservation of systemic right ventricular function. Chronic right ventricular dysfunction in patients with SV hearts may reflect irreversible adverse remodeling that is presumably a precursor to HF.[19] Unfortunately, how the systemic RV adapts to the chronically altered hemodynamic conditions of SV physiology is poorly understood, and this lack of mechanistic understanding limits the ability to identify clinically relevant pathways, biomarkers of disease progression, and effective therapeutics. The use of proven adult HF therapies has been ineffective in preventing the development of ventricular dysfunction and the progression to end-stage HF in patients with SV CHD, a finding suggesting that focused study of the mechanisms underlying HF progression in patients with SV is warranted.[13-16]

At present, very little is known about gene expression changes and cardiometabolic adaptations specific to the pediatric SV heart. Here, we performed comprehensive multiomics analysis (transcriptomics, metabolomics, and lipidomics) of the SV myocardium from both failing SV (SVHF) subjects and nonfailing SV (SVNF) subjects, compared with biventricular nonfailing (BVNF) control subjects. Furthermore, on the basis of our integrated pathway analysis, we assessed functional components of mitochondrial bioenergetics in each of these groups of patients. We

uncovered a distinct cardiometabolic profile in SVHF subjects, accompanied by altered tricarboxylic acid (TCA) cycle flux, significantly decreased mitochondrial carnitine palmitoyltransferase (CPT) enzyme activity, and mitochondrial dysfunction. Additionally, similar analysis of SVNF subjects (normal systolic function) revealed an intermediate phenotype, with less dramatic metabolic remodeling, suggesting vulnerability of the SV heart even before the onset of overt HF. Therefore, these findings may assist in the identification of new treatments aimed at preserving cardiac bioenergetics and preventing further cardiometabolic remodeling for the treatment or prevention of SV failure.

METHODS

HUMAN SUBJECTS. These studies were conducted according to Declaration of Helsinki principles. Subjects or guardians of subjects less than 18 years of age included in this study gave written informed consent before inclusion in the study, and they donated their heart tissue to the Institutional Review Board-approved pediatric and adult tissue banks at the University of Colorado Denver Anschutz Medical Campus (Aurora, Colorado, USA). Subjects included in this study were male and female patients of all ethnic backgrounds. At the time of surgical palliation or cardiac explantation, heart tissue was immediately cooled in ice-cold oxygenated Tyrode's solution in the operating room. Ventricular tissue and septa were rapidly dissected and used immediately or were flash frozen and stored at −80 °C until further use. Samples from *BVNF subjects* originated from brain dead organ donors less than 24 years of age with normal left ventricular function (ejection fraction >50%) whose hearts could not be placed because of the lack of an appropriate recipient (eg, size or blood type mismatch). Given the limited availability of fresh pediatric BVNF tissue samples, BVNF patients less than 67 years of age were included for high-resolution respirometry studies *only*, where fresh tissue was needed. RV tissue from *SV subjects* originated from patients undergoing the Norwood-Sano surgical palliation procedure or cardiac transplantation at less than 18 years of age, with a morphologic single RV and no clinical evidence of inherited cardiomyopathies. *SVNF subjects* were free from HF symptoms and had normal systolic function at the time of primary transplantation or at the time of the Norwood-Sano procedure. *SVHF subjects* underwent cardiac transplantation secondary to the presence of medically refractory HF. SVHF subjects had decreased right ventricular systolic function on transthoracic echocardiogram, medically refractory protein-losing enteropathy, plastic bronchitis, and/or right ventricular end-diastolic pressure or pulmonary capillary wedge pressure of ≥12 mm Hg. Determination of systolic function was made on the basis of review of the clinical echocardiographic report for each subject. For the purposes of some analyses, SVHF subjects were further subdivided into those with reduced systolic function on echocardiogram (SVHFrEF) and those with preserved systolic function on echocardiogram (SVHFpEF).

RNA EXTRACTION. Human RV samples were homogenized in QIAzol (Qiagen), and RNA was extracted using the RNeasy Plus Mini Kit (Qiagen). Following extraction, RNA was treated with TURBO DNase (Thermo Fisher Scientific) according to the manufacturer's protocol.

TRANSCRIPTOMIC ANALYSIS. Library preparation was performed using the TruSeq Ribo-Zero rRNA depletion kit (Illumina), and 2 × 150 total RNA sequencing was performed on an Illumina HiSEQ 4000 sequencer (high-throughput mode), with an average of 39 to 44 million mapped reads per sample. Samples were de-multiplexed and aligned to the reference genome *Homo sapiens* (hg19) using GSNAP (Genomic Short-read Nucleotide Alignment Program).[20] HTSeq software (Huber Group) was used to produce gene counts for each of our 27 samples, including RV myocardium from BVNF (n = 4), SVNF (n = 8), SVHFrEF (n = 9), and SVHFpEF (n = 6) subjects.[21] Counts of reads generated by HTSeq were normalized and annotated using the edgeR pipeline (Bioconductor).[22] Although RNA sequencing (RNA-Seq) identified more than 41,000 genes, counts of ≥5 in any 1 sample and a $\log_2$ fold-change ≥1.2 were necessary for inclusion. After filtering, approximately 7,500 to 12,000 genes remained in each data set. Significant changes in gene expression between BVNF and SVNF were calculated using Welch's *t*-test and a false discovery rate-adjusted *P* value, q <0.1. Significant changes in gene expression among the BVNF, SVHFrEF, and SVHFpEF groups were calculated using an analysis of variance (ANOVA) and post hoc false discovery rate-adjusted *P* value, q <0.1. A schematic overview of the transcriptomic analysis is provided in **Figures 1A and 1B**.

Hierarchical clustering, heat map, volcano, chord, and principal component analysis (PCA) plots were generated using R software (R Foundation). Significantly differentially regulated genes were subjected to Gene Ontology (GO) categorization,[23] canonical pathway, and gene networks analysis using Ingenuity Pathway Analysis[24] (Qiagen) and Metascape.[25]

FIGURE 1 Overview of Single-Ventricle Transcriptomic Analysis

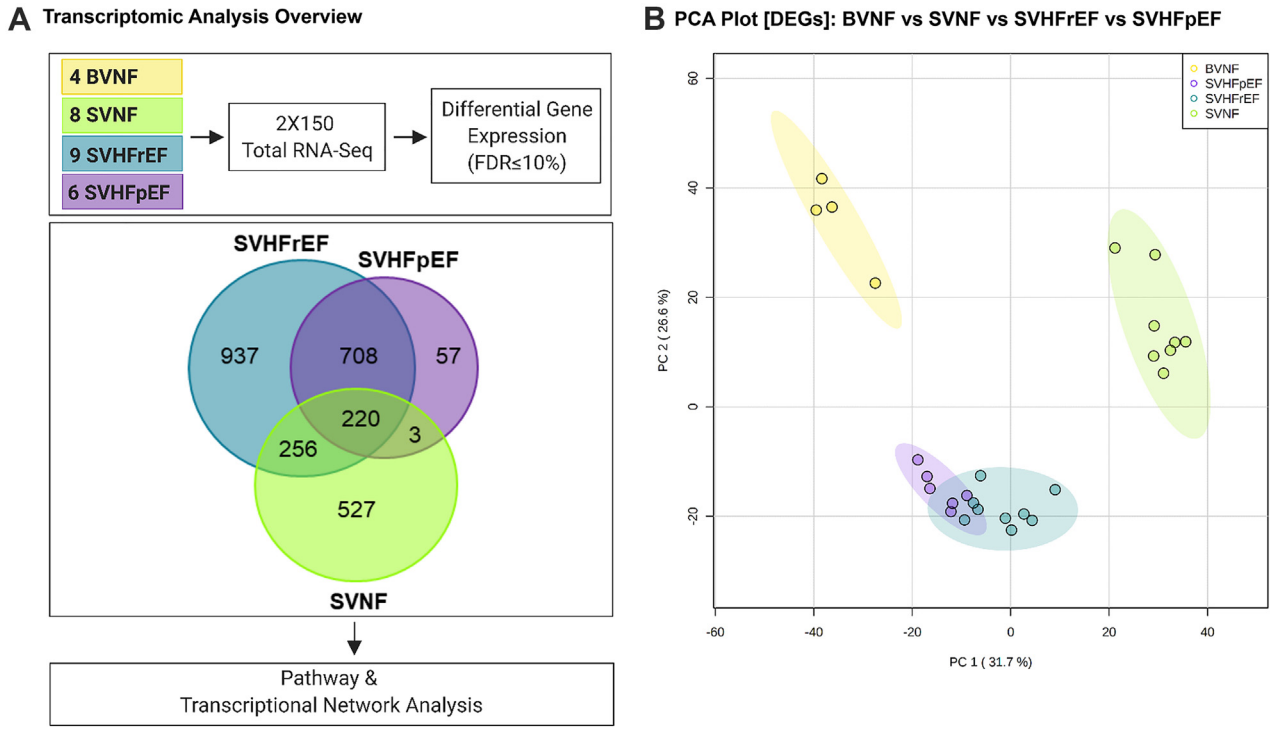

(A) Schematic overview of next-generation RNA sequencing (RNA-Seq) in biventricular nonfailing (BVNF) and single-ventricle myocardial samples. **(B)** Unbiased principal component analysis (PCA, using a combination of significantly dysregulated genes in each group relative to biventricular nonfailing samples) illustrates segregation of biventricular nonfailing, single-ventricle nonfailing (SVNF), and single-ventricle heart failure groups among the principal components and overlap between the single-ventricle heart failure with reduced ejection fraction (SVHFrEF) and single-ventricle heart failure with preserved ejection fraction (SVHFpEF) groups. DEG = differentially expressed gene; FDR = false discovery rate; PC = principal component.

Disease-gene association analyses were performed using DisGeNET (a Cytoscape application).[26,27] GO categorization of differentially expressed genes on the basis of molecular function, biologic process, and cellular component was generated using PANTHER (Protein Analysis Through Evolutionary Relationships).[28-31]

METABOLOMICS ANALYSIS. Untargeted metabolomics analysis was performed by University of Colorado Metabolomics Core Facility by using ultrahigh-pressure (UP) liquid chromatography (LC; UPLC) coupled to online mass spectrometry (MS). Briefly, cardiac tissue sample extracts were injected into a UPLC system (Ultimate 3000, Thermo) and run on a Kinetex XB-C18 column (150 × 2.1 mm and 1.7-μm particle size, Phenomenex) at 250 μL/min (mobile phase, 5% acetonitrile, Sigma-Aldrich), 95% 18 mΩ H_2O (Sigma-Aldrich), and 0.1% formic acid (Sigma-Aldrich). The UPLC system was coupled online with a Q Exactive system (Thermo), scanning in Full MS mode (2 microscans) at a 70,000 resolution in the 60- to 900-m/z range, 4-kV spray voltage, 15 sheath gases and 5 auxiliary gases, operated in negative-ion and then positive-ion mode (separate runs). Calibration was performed before each analysis against positive-ion or negative-ion mode calibration mixes (Pierce, Thermo Fisher) to ensure subparts per million error of the intact mass. Metabolite assignments were performed using Maven software,[32] on conversion of .raw files into .mzXML format through MassMatrix software. Such software allows peak picking, feature detection, and metabolite assignment against the KEGG (Kyoto Encyclopedia of Genes and Genomes) pathway database to be conducted. Assignments were further confirmed against chemical formula determination (as gleaned from isotopic patterns and accurate intact mass), and retention times were confirmed against an in-house validated standard library (>650 compounds, including

various metabolites, amino acids [AAs], and acylcarnitines) (Sigma-Aldrich; MLSMS, IROATech). Relative quantitation was performed by exporting integrated peak area values into Excel (Microsoft) for statistical analyses. To account for variability between 2 different MS runs, metabolites were normalized to the average of all BVNF control samples in each run.

PCA plots were generated using R software (R Foundation). Differentially regulated metabolites were subjected to GO categorization, canonical pathway, and networks analysis using Reactome[33-37] and MetaboAnalyst (R Foundation)[38-40] resources.

INTEGRATED MULTIOMICS ANALYSIS. Differentially regulated transcripts and metabolites were subjected to joint pathway integrated -omics analysis using the R software package MetaboAnalyst version 4.0.[38-40]

CANONICAL PATHWAY ENRICHMENT AND GENE-DISEASE ASSOCIATION ANALYSIS. Quantitative analysis of categorical data identified the pathways and molecular interactions that were most significantly enriched in differentially expressed genes, metabolites, or a combination of the 2. Fisher's exact tests were performed to calculate a P value determining the probability that the association between the genes or metabolites in the observed values and the canonical pathway are explained by chance alone. Significant enrichment was set a priori at $P < 0.05$.

CARNITINE PALMITOYLTRANSFERASE ACTIVITY. CPTI and CPTII activity was measured in RV myocardial tissue samples by using a stable isotope-based assay with carbon-14 (14C) carnitine, as described.[41] Briefly, CPTI activity is measured by permeabilizing the plasma membrane and measuring the production of palmitoyl-carnitine from palmitoyl-coenzyme A (CoA). CPTII activity is measured by permeabilizing the inner mitochondrial membrane and adding malonyl-CoA to inhibit CPTI.

HIGH-RESOLUTION RESPIROMETRY. High-resolution respirometry was conducted using the Oroboros Oxygraph-2k (O2k, Oroboros Instruments) to measure respiration in permeabilized cardiac fibers as described.[42] All O2k analyses were conducted using freshly isolated RV, LV, or septal myocardial tissue within 2 to 16 hours after explantation. Briefly, pieces of tissue were teased and placed into ice-cold biopreservation medium (BIOPS, containing 2.77 mM dipotassiocalcium ethylene glycol tetraacetic acid [EGTA], 7.23 mM dipotassium EGTA, 20 mM imidazole, 20 mM taurine, 50 mM 4-morpholine-ethanesulfonic acid, 0.5 mM dithiothreitol, 6.56 mM magnesium chloride hexahydrate, 5.77 mM disodium adenosine triphosphate (ATP), and 15 mM disodium phosphocreatine) containing 30 mg/mL saponin for 30 minutes to permeabilize the plasma membrane (all reagents from Sigma-Aldrich). Following permeabilization, samples were washed for 10 minutes in ice-cold mitochondrial respiration medium (MiR05 [Oroboros], 0.5 mM EGTA, 3mM magnesium chloride hexahydrate, 60 mM potassium lactobionate, 20 mM taurine, 10 mM potassium dihydrogen phosphate, 20 mM HEPES [4-(2-hydroxyethyl)-1-piperazineethanesulfonic acid], 110 mM sucrose, and 1 g/L fatty acid (FA)–free bovine serum albumin in sterile water; all reagents from Sigma-Aldrich) supplemented with 25 mM blebbistatin (Millipore Sigma). Samples were then blotted on filter paper, weighed, and placed into the O2k chambers containing 25 mM blebbistatin and MiR05 at 37 °C. The chambers were calibrated and mitochondrial respiratory function was measured using a stepwise substrate-uncoupler-inhibitor titration (SUIT) protocol (5 mM pyruvate, 1 mM malate, 4 mM adenosine diphosphate [ADP], 10 mM glutamate, 10 mM succinate, 10 mM cytochrome c, 0.5 mM steps of carbonyl cyanide p-trifluoromethoxyphenylhydrazone [CCCP], and 2 mM rotenone; all reagents from Sigma-Aldrich). Oxygen flux rate and oxygen concentration were simultaneously measured, and data were analyzed using DatLab software (Oroboros Datlab Version 7.0, Oroboros Instruments).

LIPIDOMIC ANALYSIS. Acyl-Coenzyme A. Acyl-CoAs were isolated from RV myocardial tissue samples as described,[43] and they were quantified by LC-MS using an API 4000 electrospray ionization mass spectrometer (AB Sciex) and an Acquity UPLC Hydrophilic Interaction Chromatography (HILIC) column (Waters) with solvent A composed of 2% ammonium hydroxide in 50% methanol and solvent B composed of 5 mM ammonium formate in methanol, pH 5. Runs were 12 minutes long with flow starting at 90% B, decreasing to 20% B at 2 minutes, and then back up to 90% B at 9 minutes. Samples were detected using neutral loss at m/z 507 and were quantified using the ratio to 3 internal standards of different chain lengths for short-, medium-, and long-chain acyl-CoAs (^{13}C-acetyl CoA, ^{13}C-C8:0 CoA, and C17:0 CoA, respectively; Avanti Polar Lipids).[43]

Sphingolipids. Sphingolipids were isolated from RV myocardial tissue samples, extracted onto a 1-phase neutral organic solvent system, and analyzed by LC-MS-MS on an API-2000 mass spectrometer using ceramide standards (Avanti Polar Lipids) to identify

both nonpolar and polar species as described.[44,45] Sphingolipid species were quantified per milligram of protein on the basis of a protein assay of the tissue homogenates (BCA Protein Assay Kit, Pierce).

Phospholipids. Phospholipids were extracted from RV myocardial tissue samples that were homogenized using a glass-on-glass homogenizer in phosphate-buffered saline (PBS) according to previously published methods.[46-48] Phospholipids were quantified using LC coupled to electrospray ionization MS in an API 4000 mass spectrometer, as described.[49] Tetramyristyl cardiolipin (1,000 nmol) and Splash phospholipid standards (Avanti Polar Lipids) were used as internal standards to identify phospholipid retention times. Phospholipid species were quantified per milligram of protein on the basis of a protein assay of the tissue homogenates (BCA Protein Assay Kit). Analysis was performed using Analyst software.

STATISTICAL ANALYSIS. With the exception of the transcriptomic analysis, all statistical analyses were performed using GraphPad Prism version 9.0 (GraphPad Software), and statistical significance was set a priori at $P < 0.05$. All statistical tests used and graphic depictions of data (means and error bars, or box and whisker plots) are defined within the figure legends for the respective data panels. Exact n values for all experiments with statistical analysis are included in the figure legends. Data were tested for gaussian distribution with the Shapiro-Wilk normality test. Welch's correction was used when variances were unequal on the basis of the F-test. Comparisons between 2 normally distributed groups were conducted using an unpaired *t*-test, comparisons between 2 non-normally distributed groups were conducted using the nonparametric Mann-Whitney test, and comparisons between 2 groups with unequal variances were conducted using Welch's *t*-test. Comparisons of 3 or more normally distributed groups were conducted using a 1-way ANOVA; if the overall comparison reached significance, a Holm-Sidak post hoc test for multiple pairwise comparisons was performed. Comparisons among 3 or more non-normally distributed groups were conducted using the nonparametric Kruskal-Wallis test; if the overall comparison reached significance, Dunn's post hoc test for multiple pairwise comparisons was performed. Comparisons among 3 or more groups with unequal variances were conducted using Welch's ANOVA; if the overall comparison reached significance, Dunnett's post hoc test for multiple pairwise comparisons was performed.

RESULTS

SUBJECT CHARACTERISTICS. Aggregate characteristics for patients included in this study are listed in **Table 1**, and a more detailed description of individual subject characteristics is included in Supplemental Table 1**.** A total of 32 BVNF, 21 SVNF, and 34 SVHF (n = 26, SVHFrEF; n = 8, SVHFpEF) subjects were included in this study. Given the amount of tissue required for each experiment combined with the finite resource the tissue bank represents, all analyses could not be performed on every patient. Therefore, for those studies relying on frozen tissue (eg, RNA-Seq, CPT activity, metabolomics, and lipidomics), inclusion in the study was determined on the basis of the amount of tissue available for use.

DISTINCT TRANSCRIPTOMIC PROFILES DISCRIMINATE SINGLE-VENTRICLE HEART DISEASE SUBJECTS FROM CONTROL SUBJECTS. Next generation RNA-Seq was performed on RV myocardial tissue samples from BVNF (n = 4), SVNF (n =8), and SVHF (SVHFrEF, n = 9; SVHFpEF, n = 6) patients. A schematic overview of the comprehensive transcriptomic analysis is provided in **Figure 1A**, with segregation of groups on the basis of phenotype evident in the PCA seen in **Figure 1B**. There were 1,007 significantly differentially expressed genes (DEGs) between BVNF and SVNF myocardial samples. Of these, roughly one-half (477) were up-regulated, whereas the remaining 530 were down-regulated (**Figure 2A**; the top 20 DEGs are listed in the volcano plot). Unsupervised hierarchical clustering separated BVNF and SVNF subjects on the basis of their DEG profiles (**Figure 2B**). A list of all 1,007 DEGs is included in Supplemental Table 2. Gene-disease association analysis performed using DisGeNET[26,27,50] on DEGs predicted dysregulated disease processes, including liver amyloidosis, fatty liver disease, complement deficiency, and atrial septal defects associated with SVNF samples (**Figure 2C**). Pathway and transcriptional network analysis performed using a combination of Ingenuity Pathway Analysis and Metascape revealed multiple dysregulated canonical pathways associated with SVNF samples (**Figure 2D**). Most prominently, canonical pathways involved in the immune and inflammatory response, cell cycle, lipid metabolism, signaling, and development were significantly enriched ($P < 0.01$) in SVNF samples relative to BVNF control subjects. PANTHER GO analysis was used to categorize the 1,007 DEGs on the basis of their implicated functional processes. The top 3 biologic process categorizations

TABLE 1 Aggregate Characteristics for All Subjects Included in This Study

Experiment (Figure)	Group	N	Sex, % Male	Age, Median Years (Q1-Q3)	Last Surgical Palliation
RNA-Seq (Figures 1-4)	BVNF	4	50	2.32 (1.38-4.18)	–
	SVNF	8	38	0.23 (0.11-0.23)	N = 4 none, n = 3 PDA stent, bilateral PA bands
	SVHF	15	60	3.85 (1.92-7.23)	N = 4 Norwood, n = 4 Glenn, n = 7 Fontan
CPT Activity (Figure 5)	BVNF	10	80	10.83 (1.3-18.00)	–
	SVNF	4	50	0.22 (0.1-0.27)	N = 4 PDA stent
	SVHF	13	54	2.92 (0.3-6.70)	N = 4 Norwood, n = 6 Glenn, n = 3 Fontan
O2k (Figure 5)	BVNF	15	33	53 (5-56.5)	–
	SVNF	8	75	0.01 (0.005-0.06)	N = 8 none
	SVHF	14	79	5.65 (0.23-9.93)	N = 2 Norwood, n = 4 Glenn, n = 1 hemi-Fontan, n = 7 Fontan
Metabolomics (Figures 6 and 7)	BVNF	10	60	7.70 (4.18-8.67)	–
	SVNF	5	40	0.23 (0.20-0.40)	N = 5 PDA stent, bilateral PA bands
	SVHF	10	50	2.45 (1.06-4.56)	N = 1 PDA stent, bilateral PA bands, n = 3 Norwood, n = 4 Glenn, n = 2 Fontan
All patient samples	BVNF	32	53	17.5 (1.3-52.25)	–
	SVNF	21	52	0.13 (0.005-0.24)	N = 6 PDA stent, n = 2 PDA stent, bilateral PA bands, n = 13 none
	SVHF	34	68	3.9 (0.23-7.40)	N = 2 PDA stent, bilateral PA bands, n = 7 Norwood, n = 9 Glenn, n = 1 hemi-Fontan, n = 14 Fontan, n = 1 Kawashima

BVNF = biventricular nonfailing; CPT = carnitine palmitoyltransferase; O2k = Oroboros Oxygraph-2k (Oroboros Instruments); PA = pulmonary artery; PDA = patent ductus arteriosus; Q1-Q3 = 25th-75th percentiles; RNA-Seq = RNA sequencing; SVHF = single-ventricle heart failure; SVNF = single-ventricle nonfailing.

indicated that most of the DEGs are involved in cellular processes (25.4%, eg, cell communication, activation, division), biologic regulation (14.6%; eg, regulation of biologic processes, quality, and molecular function), and metabolic processes (14.5%; eg, primary metabolism and ATP metabolism) (Figure 2E).

RNA-Seq was also performed on RV myocardial tissue samples from a subset of SVHF patients (n = 15, SVHF; n = 9, SVHFrEF; and n = 6, SVHFpEF) (Figures 1A and 1B). There were 928 DEGs shared between SVHFrEF and SVHFpEF groups (Figure 3A). Of these, 634 were up-regulated, whereas 294 were down-regulated (Figure 3B). Unsupervised hierarchical clustering separated BVNF and SVHF subjects on the basis of DEGs (Figure 3C). A list of all 928 DEGs is included in Supplemental Table 3. Gene-disease association analysis of the 928 DEGs predicted dysregulated disease processes, including infection, liver cirrhosis, myopathy, immune disease, and decreased mitochondrial activity associated with SVHF samples (Figure 3D). Pathway and transcriptional network analysis revealed multiple dysregulated canonical pathways associated with SVHF (Figure 3E). Most prominently, canonical pathways involved in the immune and inflammatory response, translation, mitochondrial metabolism, RNA metabolism, and autophagy were significantly enriched (P <0.01) in SVHF subjects relative to BVNF control subjects. The top 3 biologic process categorizations indicated that most of the 928 DEGs are involved in cellular processes (30.8%; eg, cell activation, communication, division), metabolic processes (19.2%; eg, primary metabolism and ATP metabolism), and biologic regulation (15.4%; eg, regulation of biological processes, quality, and molecular function) (Figure 3F).

There were 220 common DEGs between the SVNF and SVHF groups, a finding suggesting that these genes are associated with SV regardless of HF status (Figure 4A and Supplemental Figures 1A and 1B). Pathway and transcriptional network analysis of those 220 common DEGs identified the immune response and various signaling pathways as conserved across all SV samples (Supplemental Figures 1A and 1B). Additionally, there were 708 DEGs specifically associated with SVHF. Pathway and transcriptional network analysis of those 708 SVHF-specific DEGs identified mitochondrial metabolism and RNA metabolism as significantly dysregulated (P <0.01) specifically in SVHF subjects (Figures 4A and 4B). A list of all 220 common DEGs and all 708 SVHF-specific DEGs are included in Supplemental Tables 4 and 5, respectively.

MITOCHONDRIAL BIOENERGETICS ARE IMPAIRED IN SINGLE-VENTRICLE MYOCARDIUM. Because long-chain FAs are well recognized as the preferred substrate for oxidative phosphorylation (OXPHOS) by cardiac mitochondria,[51] we quantified the activity of the mitochondrial CPT system that is required for the delivery of long-chain FAs from the cytoplasm into the mitochondria for their subsequent β-oxidation

FIGURE 2 Distinct Transcriptomic Profiles Discriminate Nonfailing Single-Ventricle Subjects From Control Subjects

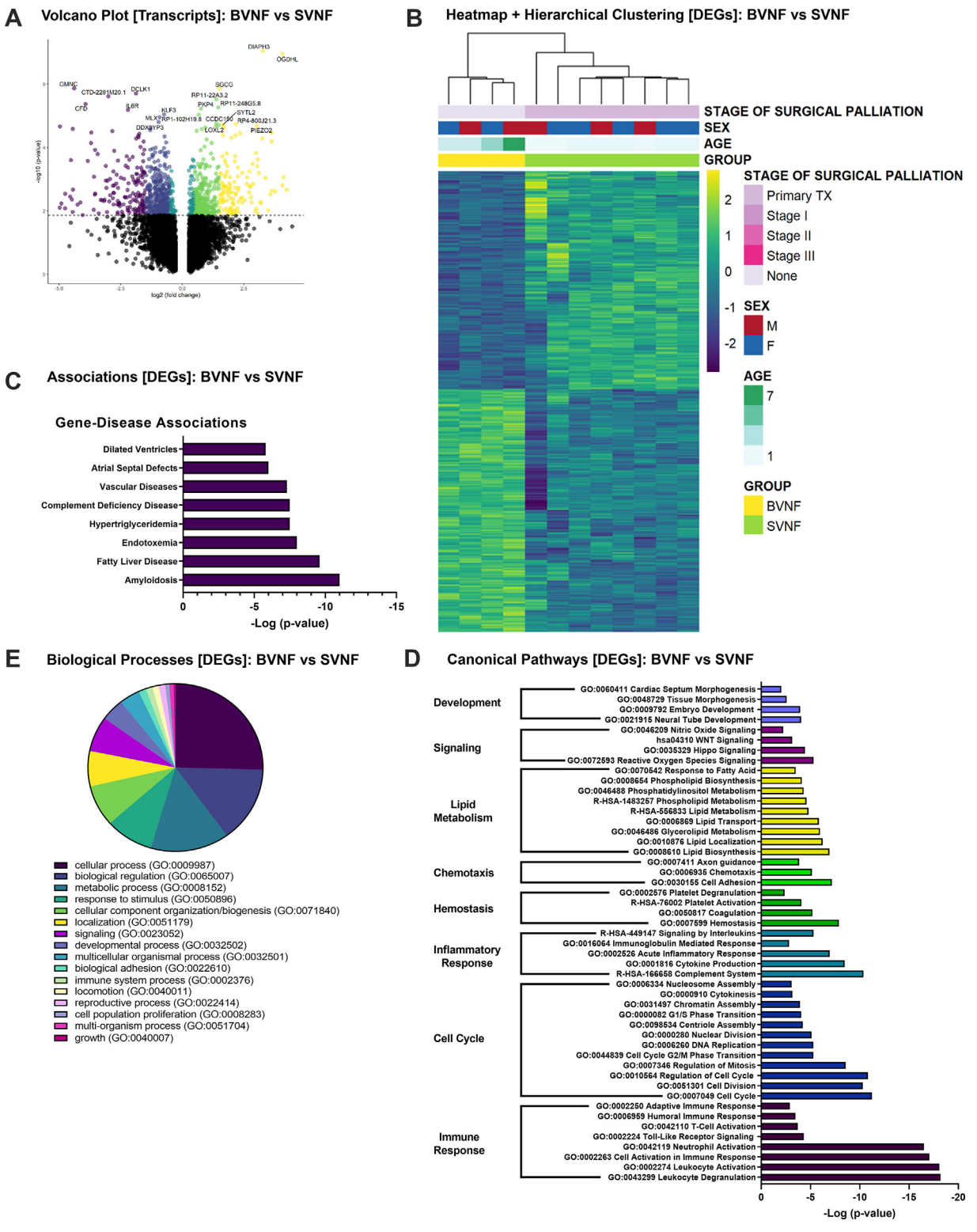

Continued on the next page

(β-OX) (Figure 5A). The enzymatic activity of CPTI and CPTII was significantly decreased ($P = 0.018$ and $P = 0.013$, respectively) in SVHF myocardial tissue compared with BVNF tissue (Figure 5B). Additionally, although CPTI activity is preserved in the SVNF heart, the activity of CPTII is significantly decreased ($P = 0.007$) compared with BVNF tissue (Figure 5B).

Additionally, we quantified mitochondrial function by using high-resolution respirometry to assess OXPHOS capacity in a subset of BVNF, SVNF, and SVHF freshly isolated myocardial fibers (a representative sample trace is shown in Figure 5C). There was significantly lower normalized mitochondrial oxygen flux in SVHF myocardium using pyruvate, malate, and ADP (complex [C] I), glutamate (CI), and succinate (CI and CII) as substrates ($P = 0.044$, $P = 0.019$, and $P = 0.014$, respectively) (Figure 5D). Additionally, there was significantly lower maximal respiration in SVHF with bypassing of oxygen flux through CI and CII using the uncoupler carbonyl cyanide m-chlorophenyl hydrazone (CCCP; $P = 0.004$). Oxygen flux was also measured in SVNF myocardial samples, and although there were trends toward decreased CI activity, we noted no statistically significant changes in CI, CI and CII, or maximal respiratory capacity in SVNF subjects (Figure 5D).

SINGLE-VENTRICLE MYOCARDIUM IS ASSOCIATED WITH IMPAIRED MITOCHONDRIAL, AMINO ACID, AND LIPID METABOLISM. Given the significant overrepresentation of genes associated with mitochondrial metabolism and the pathologic changes in mitochondrial function seen in SVHF subjects, metabolomics analysis was conducted on myocardial tissue samples from a subset of BVNF, SVNF, and SVHF patients. Unbiased PCA separated SVNF from BVNF subjects (Figure 6A) and SVHF from BVNF subjects (Figure 6D) on the basis of their significantly differentially expressed metabolites (DEMs). Reactome-based pathway analysis of all DEMs revealed canonical pathways similar to those detected by transcriptomic analysis alone. Pathways related to the cell cycle, AA metabolism, and transport, for example, were significantly dysregulated ($P < 0.05$) in SV myocardium (Figures 6B and 6E).

Molecular pathway and network analysis of both DEGs and DEMs was performed using MetaboAnalyst. Integrated multiomics analysis revealed multiple overlapping dysregulated pathways associated with SV, similar to those identified in each data set alone (Figures 6C and 6F). Most notably, pathways implicated in AA metabolism, the TCA cycle, the immune system, lipid metabolism, and RNA metabolism were significantly enriched ($P < 0.05$) in SV samples relative to BVNF control subjects on the basis of DEG and DEM profiles.

On the basis of the overrepresentation of lipid and mitochondrial metabolic pathways related to SVHF in the integrated multiomics analysis, specific metabolites associated with the TCA cycle were assessed in more detail (Figure 7A). Although there were no significant changes in metabolites related to glycolysis (glucose, glucose 6-phosphate, pyruvate, or lactate), the fundamental metabolite, citrate, and the TCA cycle intermediate, α-ketoglutarate, were significantly increased in SVNF ($P = 0.008$ and $P = 0.017$, respectively) and SVHF ($P = 0.046$ and $P = 0.046$, respectively) myocardial samples relative to BVNF control subjects. TCA cycle intermediates succinate, fumarate, malate, cofactor nicotinamide adenine dinucleotide (NAD^+), and ADP, however, were significantly decreased ($P = 0.049$, $P = 0.028$, $P = 0.041$, $P = 0.049$, and $P = 0.026$, respectively), specifically in SVHF samples relative to BVNF control subjects. Importantly, energy molecules ATP ($P = 0.039$) and phosphocreatine ($P = 0.034$) were

FIGURE 2 Continued

(A) Volcano plot representation of all the transcripts detected (after filtering) by RNA sequencing depicted as the $\log_2$ fold-changes in expression (x-axis) and the log odds of a gene being differentially expressed (y-axis), thus highlighting the 1,007 transcripts that are significantly differentially expressed between biventricular nonfailing (BVNF) and single-ventricle nonfailing (SVNF) samples **(above dotted line);** Welch's *t*-test, false discovery rate-adjusted *P* value of q <0.1 (*P* <0.01). **(B)** Heat map of the 1,007 significantly differentially expressed transcripts in single-ventricle nonfailing myocardium (raw fragments per kilobase of transcript per million mapped reads [FPKM values]). Unsupervised hierarchical clustering separated biventricular nonfailing (n = 4) and single-ventricle nonfailing (n = 8) patient samples. **(C)** Significantly dysregulated associations in biventricular nonfailing vs single-ventricle nonfailing samples identified with DisGeNET by using the 1,007 transcripts that changed significantly in single-ventricle nonfailing samples (*P* <0.01, a minimum count of 3, and an enrichment factor >1.5). **(D)** Significantly dysregulated canonical pathways in biventricular nonfailing vs single-ventricle nonfailing samples identified with Ingenuity Pathway Analysis and Metascape by using the 1,007 transcripts that changed significantly in single-ventricle nonfailing samples (Fisher's exact test, $-\log_{10}$ [*P* value] >1.3 or *P* <0.05). **(E)** Categorization of Gene Ontology (GO) annotations for biologic processes in biventricular nonfailing vs single-ventricle nonfailing right ventricular myocardial samples identified with PANTHER (Protein Analysis Through Evolutionary Relationships) by using the 1,007 transcripts that changed significantly in single-ventricle nonfailing samples. DEG = differentially expressed gene; R-HSA = Reactome Gene Sets - Homo Sapiens; TX = transplantation.

FIGURE 3 **Distinct Transcriptomic Profiles Discriminate Failing Single-Ventricle Subjects From Control Subjects**

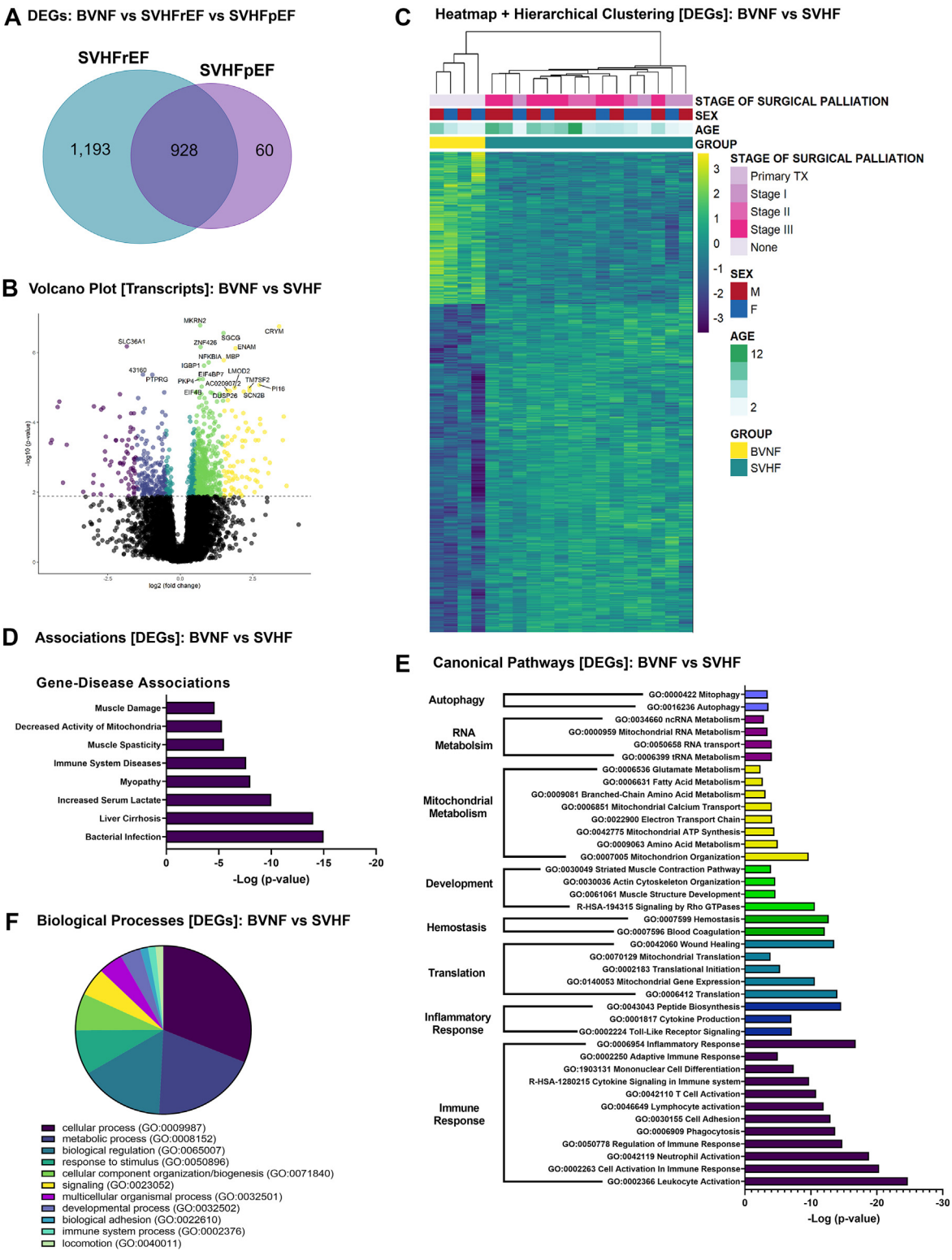

Continued on the next page

also significantly decreased in SVHF myocardial samples relative to BVNF control samples. Moreover, whereas ATP levels were preserved in SVNF subjects, phosphocreatine was significantly decreased ($P = 0.019$).

Given the implication of alterations in AA metabolism in SVHF, all AAs detected by metabolomics analysis were assessed in more detail (**Figure 7B**). Numerous AAs, including alanine, asparagine, aspartate, glycine, histidine, methionine, phenylalanine, proline, and serine, were significantly decreased ($P < 0.001$, $P = 0.003$, $P = 0.048$, $P = 0.001$, $P < 0.001$, $P < 0.001$, $P = 0.007$, $P = 0.030$, and $P = 0.021$, respectively) in SVHF myocardial samples compared with BVNF samples. Strikingly, however, the branched-chain AA (BCAA) isoleucine was significantly increased (more than 540-fold; $P < 0.001$) in SVHF samples relative to BVNF control samples. Several AAs, including asparagine, glycine, phenylalanine, and serine, were also significantly decreased in the SVNF myocardium ($P = 0.003$, $P = 0.046$, $P = 0.007$, $P = 0.021$, respectively), whereas arginine ($P = 0.014$) and the BCAAs isoleucine and valine ($P < 0.001$ and $P = 0.001$, respectively) were significantly increased (**Figure 7B**).

Moreover, given the importance of mitochondrial FA β-OX in the heart and the overrepresentation of mitochondrial metabolic pathway alterations in SVHF, lipidomic analysis of acyl-CoAs and acylcarnitines was conducted in BVNF and SVHF cardiac specimens. Although free and acetyl-CoA values were unchanged in SVHF samples, short-chain (total carbon atom numbers from 1C to 7C) acyl-CoA species were significantly increased ($P = 0.049$), whereas medium-chain (8C-15C) and long-chain (≥16C) acyl-CoA species were significantly decreased ($P = 0.038$ and $P = 0.003$, respectively) in SVHF samples relative to BVNF control samples (Supplemental Figure 2A). Correspondingly, there was no significant change detected in acetyl-L-carnitine levels, but short-chain carnitine species were significantly increased ($P = 0.005$), whereas L-carnitine, medium-chain, and long-chain carnitine species were significantly decreased ($P = 0.031$, $P = 0.025$, and $P = 0.008$, respectively) in SVHF samples relative to BVNF control samples (Supplemental Figure 2B).

Lipidomics analysis of sphingolipids identified no significant changes in ceramide, glucosylceramide, or sphingosine levels in the SVHF myocardium; however, total lactosylceramide was significantly increased in SVHF samples relative to BVNF control samples ($P = 0.007$) (Supplemental Figure 2C). Additionally, phospholipid species, including phosphatidylcholine, phosphatidylinositol, phosphatidylethanolamine, and phosphatidylglycerol, were significantly decreased in SVHF samples ($P = 0.036$, $P = 0.004$, $P < 0.001$, and $P = 0.029$ respectively) relative to BVNF control samples (Supplemental Figure 2D).

DISCUSSION

Although there are growing numbers of infants and children living with SV physiology, no previous comprehensive studies have evaluated transcriptomic, metabolomic, lipidomic, or functional changes in the SV heart. There is a major gap in knowledge related to the specific molecular changes

FIGURE 3 Continued

(A) Venn diagram of differentially expressed genes (DEGs) in each group; 928 differentially expressed genes were common among single-ventricle heart failure (SVHF) myocardial samples; 1,193 differentially expressed genes were specific to single-ventricle heart failure with reduced ejection fraction (SVHFrEF) myocardial samples; 60 differentially expressed genes were specific to single-ventricle heart failure with preserved ejection fraction (SVHFpEF) myocardial samples. **(B)** Volcano plot representation of all the transcripts detected (after filtering) by RNA sequencing depicted as the $\log_2$ fold-changes in expression (x-axis) and the log odds of a gene being differentially expressed (y-axis), thus highlighting the 928 transcripts that are significantly differentially expressed between biventricular nonfailing (BVNF) and all single-ventricle heart failure samples **(above dotted line);** analysis of variance (biventricular nonfailing vs single-ventricle heart failure with reduced ejection fraction vs single-ventricle heart failure with preserved ejection fraction groups) and post hoc false discovery rate-adjusted *P* value, q <0.1. **(C)** Heat map of the 928 significantly differentially expressed transcripts in single-ventricle heart failure myocardium (raw fragments per kilobase of transcript per million mapped reads [FPKM] values). Unsupervised hierarchical clustering separated biventricular nonfailing (n = 4) and single-ventricle heart failure (n = 15; n = 9, single-ventricle heart failure with reduced ejection fraction; n = 6, single-ventricle heart failure with preserved ejection fraction) patient samples. **(D)** Significantly dysregulated associations in biventricular nonfailing vs single-ventricle heart failure samples identified with DisGeNET using the 928 transcripts that changed significantly in all single-ventricle heart failure samples (*P* <0.01, a minimum count of 3, and an enrichment factor >1.5). **(E)** Significantly dysregulated canonical pathways in biventricular nonfailing vs single-ventricle heart failure samples identified with Ingenuity Pathway Analysis and Metascape using the 928 transcripts that changed significantly in all single-ventricle heart failure samples; Fisher's exact test, $-\log_{10}$ (*P* value) >1.3 or *P* <0.05. **(F)** Categorization of Gene Ontology (GO) annotations for biologic processes in biventricular nonfailing vs single-ventricle heart failure right ventricular myocardial samples identified with PANTHER (Protein Analysis Through Evolutionary Relationships) using the 928 transcripts that changed significantly in all single-ventricle heart failure samples. Abbreviations as in **Figure 2**.

FIGURE 4 **The Failing Single Ventricle Is Typified by Altered Metabolic Transcripts**

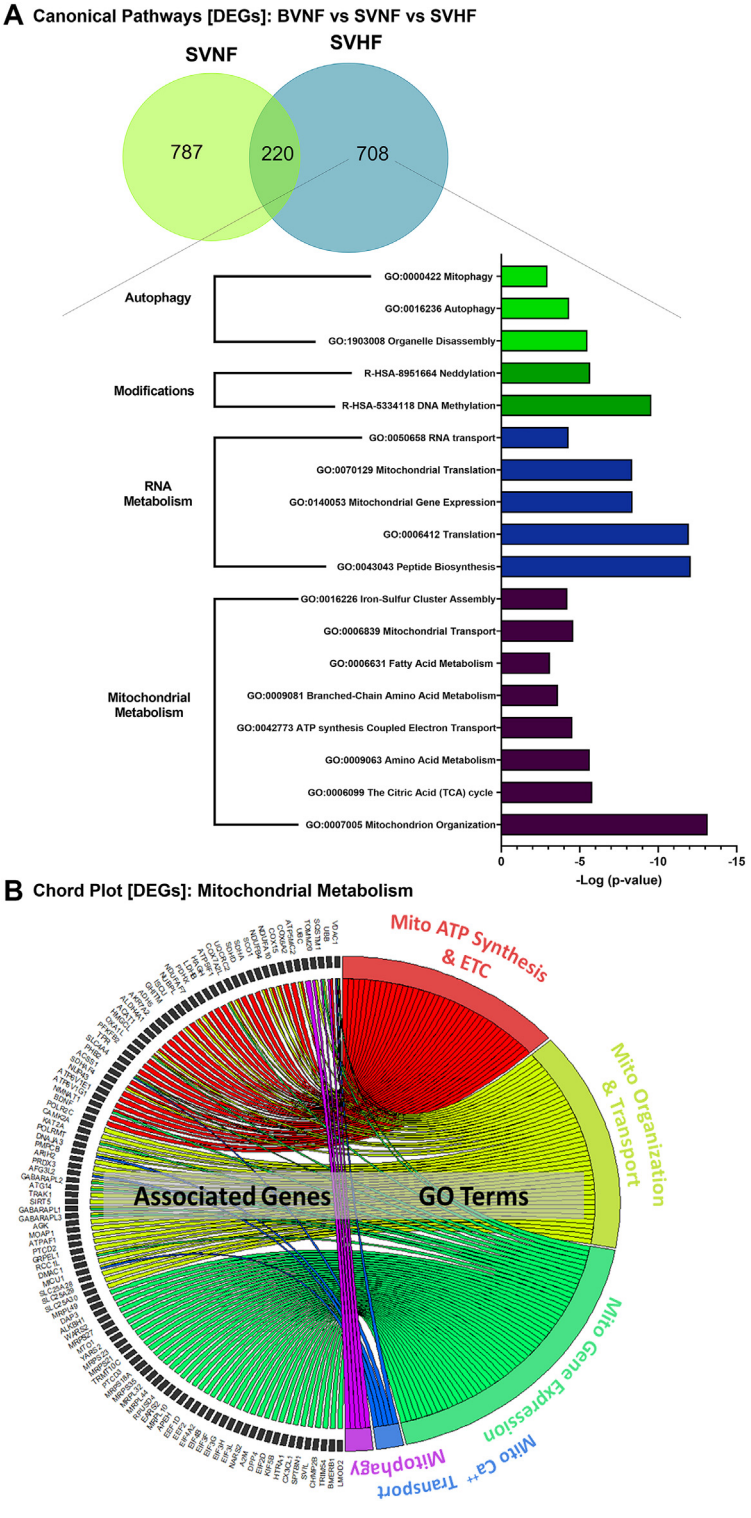

Continued on the next page

associated with adaptation and remodeling of the systemic RV, and the ability to predict the progression to HF in patients with SV has been limited, primarily by an incomplete understanding of the disease pathogenesis. This is the first study to perform comprehensive multiomic characterization of human SV myocardium in combination with functional bioenergetic analysis of the SV heart. In an effort to understand the transition to HF in patients with SV more thoroughly, we conducted our study using both SVHF and SVNF myocardial samples. This integrative approach provides important insight into the molecular remodeling of the SV heart before overt HF and identifies potential mechanisms associated with the transition to HF in this vulnerable group of patients.

Our next-generation RNA-Seq analyses revealed a common transcriptional program associated with SV that is highly enriched for alterations in immune effector pathways regardless of HF status. Of note, surgical thymectomy is performed routinely in infants with CHD during surgical repair or palliation, and although the consequences of this procedure are poorly understood, mounting evidence suggests that this practice could result in altered immune cell composition and impaired immune-mediated responses.[52,53] Additionally, investigators have shown that neonates with HLHS display evidence of inflammatory activation preoperatively as well as postoperatively, and the degree of inflammatory response correlates with postoperative outcomes and mortality.[54,55] The specific alterations in immune responses will be an interesting avenue for further investigation in patients with SV CHD, particularly in the context of metabolic remodeling.

With respect to the failing SV heart, canonical pathways related to RNA metabolism, mitochondrial metabolism, and autophagy or mitophagy were specifically overrepresented. These data demonstrate altered mitochondrial metabolic pathways as a hallmark of the failing SV myocardium. Intriguingly, some metabolic genes are up-regulated in the failing SV heart and are unchanged in the nonfailing SV heart, a finding suggesting that post-transcriptional and post-translational modifications may contribute to alterations in cardiac energy metabolism in SV CHD. A summary of the major metabolic changes in SVNF and SVHF myocardium compared with BVNF myocardium is shown in **Figure 8**.

Reducing equivalents necessary for OXPHOS are generated by FA β-OX, pyruvate oxidation, and the TCA cycle and are then delivered to the electron transport chain for ATP production. Therefore, alterations in TCA cycle intermediates suggest impaired TCA cycle flux leading to downstream impaired electron transport chain function. Here we show that in addition to alterations in metabolic gene expression, the failing SV heart is characterized by an altered abundance of TCA cycle metabolites, AAs, acyl-CoAs, acylcarnitines, phospholipids, and overall decreased myocardial energy supply (diminished ATP and phosphocreatine levels), suggesting global dysregulation of cardiac metabolism. Interestingly, although gene expression changes related to mitochondrial metabolism were not seen in the nonfailing SV heart, levels of phosphocreatine, which can be used for the maintenance and recycling of ATP in the myocardium, were significantly diminished, a finding suggesting limited myocardial energy reserve capacity even in SVNF subjects. When taken together, these data suggest that there is truncated TCA cycle flux such that levels of the more proximal intermediates (citrate and α-ketoglutarate) are elevated in both SVNF and SVHF hearts, whereas the more distal intermediates (succinate, fumarate, and malate) are decreased in SVHF. Although it was beyond the scope of this study to quantify the activity of TCA cycle enzymes such as isocitrate dehydrogenase, succinate dehydrogenase, or fumarate hydratase, this information could provide important insights into TCA cycle function in SV CHD. The TCA cycle may play an important role in the transition to HF in SV CHD, and it therefore represents a potential therapeutic target for SV failure.

In the healthy heart, long-chain FAs are well recognized as the preferred substrates for OXPHOS by cardiac mitochondria.[51,56] The mitochondrial CPT

FIGURE 4 Continued

(A) Venn diagram of differentially expressed genes (DEGs) in each group; 220 differentially expressed genes were common between single-ventricle nonfailing (SVNF) and single-ventricle heart failure (SVHF) myocardial samples; 708 differentially expressed genes were specific to single-ventricle heart failure myocardial samples; 787 differentially expressed genes were specific to single-ventricle nonfailing myocardial samples. Significantly dysregulated canonical pathways in biventricular nonfailing (BVNF) vs single-ventricle heart failure samples identified with Ingenuity Pathway Analysis and Metascape using the 708 heart failure–specific differentially expressed transcripts that changed significantly in only single-ventricle heart failure samples; Fisher's exact test, $-\log_{10}$ (*P* value) >1.3 or $P < 0.05$. **(B)** Chord plot illustrating the relationship between differentially expressed genes related to mitochondrial metabolism (associated genes) and each differentially expressed canonical pathway (Gene Ontology [GO] term). ATP = adenosine triphosphate; Ca^{++} = calcium; R-HSA = Reactome Gene Sets - Homo Sapiens; Mito = mitochondrial.

FIGURE 5 Mitochondrial Bioenergetics Are Impaired in Single-Ventricle Subjects

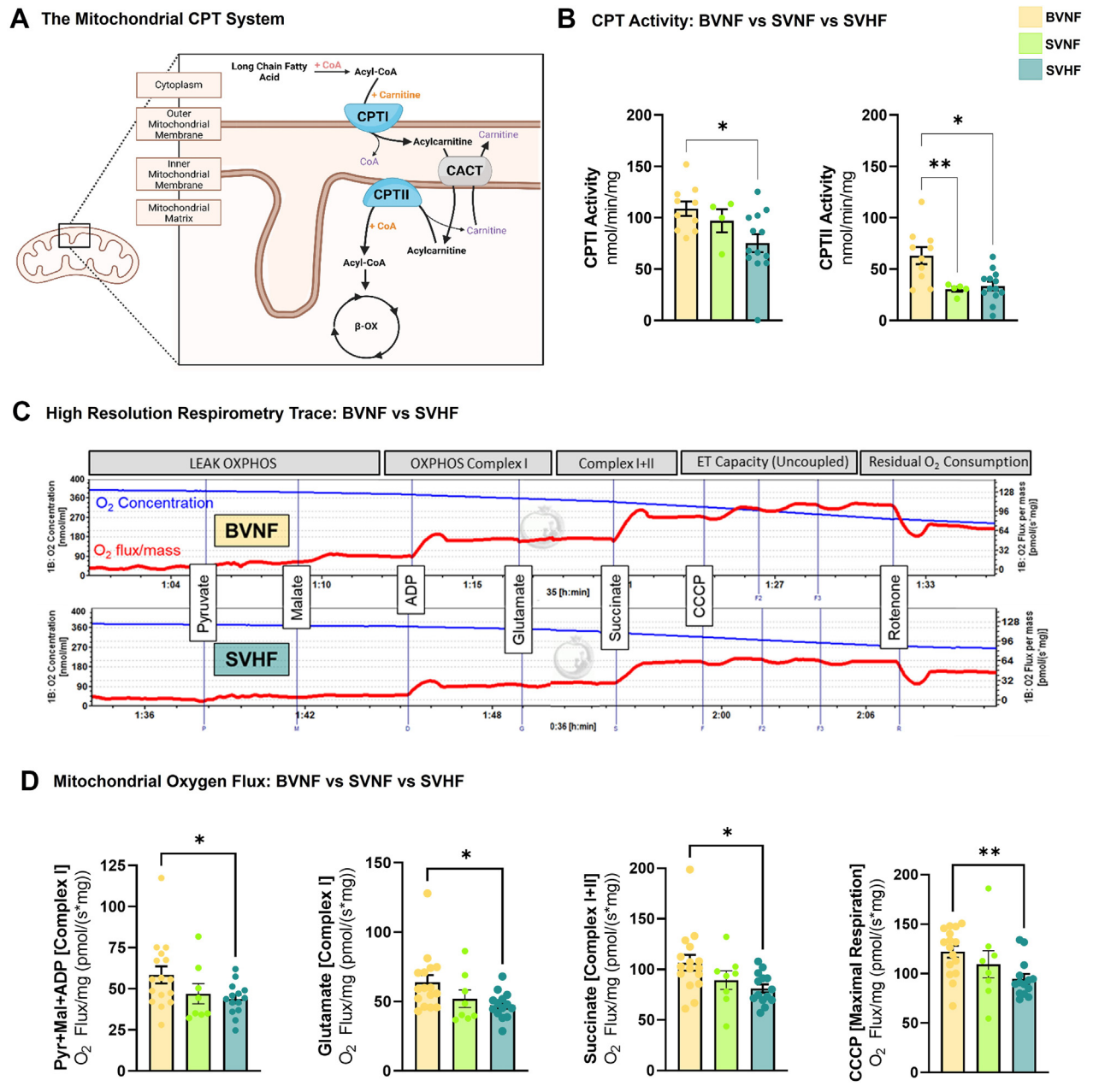

(A) Graphic illustration of the mitochondrial carnitine palmitoyltransferase (CPT) System. **(B)** Stable isotope-based enzymatic activity analysis of carnitine palmitoyltransferase I and II (CPTI and CPTII) in biventricular nonfailing (BVNF), single-ventricle nonfailing (SVNF), and single-ventricle heart failure (SVHF) myocardial samples. For all groups, box and whisker plot shows mean (bar) and minimum to maximum (ends); each point represents individual patient values (n = 10, biventricular nonfailing; n = 4, single-ventricle nonfailing; and n = 13, single-ventricle heart failure samples); **asterisks** denote significant differences among groups; **P* <0.05 and ***P* <0.01; analysis of variance (Welch) and Dunnett's. **(C)** Representative high-resolution respirometry trace from the Oroboros Oxygraph 2K. **(D)** Mitochondrial oxygen flux in biventricular nonfailing and single-ventricle heart failure myocardial samples. For all groups, bar equals mean ± SEM; each point represents individual patient values (n = 16 [1 patient replicate], biventricular nonfailing; n = 8 single-ventricle nonfailing; and n = 14, single-ventricle heart failure samples); **asterisks** denote significant differences among groups; **P* <0.05 and ***P* <0.01; analysis of variance and Holm-Sidak for pyruvate (Pyr) and malate (Mal) and adenosine diphosphate (ADP), Kruskal-Wallis test and Dunn's for glutamate, succinate, and carbonyl cyanide p-trifluoromethoxyphenylhydrazone (CCCP). CACT = carnitine-acylcarnitine translocase; CoA = coenzyme A; ET = electron transport; β-OX = β-oxidation; OXPHOS = oxidative phosphorylation.

FIGURE 6 **Metabolic and Signaling Pathways Are Dysregulated in Single-Ventricle Subjects**

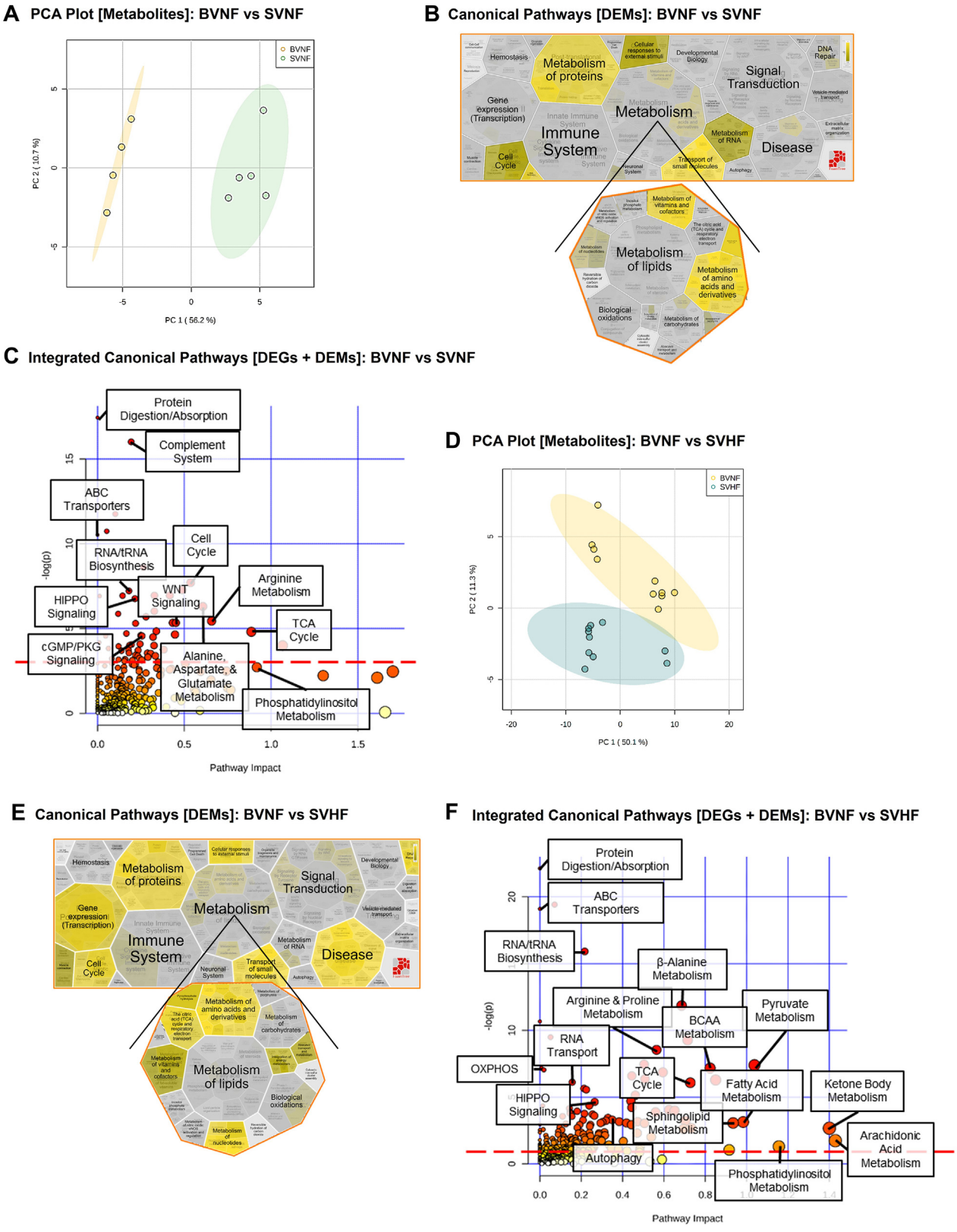

Continued on the next page

system is responsible for the delivery of long-chain FAs from the cytoplasm into the mitochondria for their subsequent oxidation,[57] and CPTI catalyzes the rate-limiting step of β-OX by converting acyl-CoAs into acylcarnitines. Functional analysis of the mitochondrial CPT system demonstrated significantly decreased activity of the mitochondrial CPT transporters, therefore suggesting that the decreased abundance of myocardial acylcarnitine species is related to an overall decreased capacity of the failing SV heart to oxidize long-chain FAs, with a resulting diminished rate of cardiac ATP production. Although we are unable on the basis of the present study to identify the mechanism by which CPT activity is significantly reduced in SVHF, these data suggest a potential increased reliance on short-chain FA oxidation in the failing SV heart. However, further work is needed to understand fully this complex system in the context of SV physiology.

Interestingly, although CPTI activity was preserved in the nonfailing SV myocardium, the enzymatic activity of CPTII was significantly reduced, thus suggesting an intermediate phenotype of bioenergetic remodeling in the nonfailing SV heart where some changes in mitochondrial bioenergetics precede development of overt HF. In addition to the role of the CPT system in activating β-OX and ATP production, this system also functionally intertwines with other key pathways and factors to regulate both gene expression and the production of potentially toxic lipid metabolites such as sphingolipids and their precursors, palmitoyl-CoA and palmitic acid. Therefore, the activity of the CPT system and the specific metabolic lipid milieu are important modulators of overall mitochondrial function, and restoration or preservation of CPT enzymatic activity could represent a novel avenue for the prevention and treatment of SVHF.

Given the critical need for a constant supply of energy in the beating heart, it is not surprising that many causes of cardiovascular disease involve disturbances in cardiac metabolism.[51,56,58] However, the systemic RV may be uniquely vulnerable to increased energy demand because morphologically it is designed to pump to the low-resistance pulmonary circulation. It is known that patients with SV have decreased exercise tolerance compared with their peers, with an aerobic capacity 66% of that in the healthy population,[59] consistent with altered myocardial energetics in SV physiology. We also previously showed that although the failing SV heart has no significant change in relative mitochondrial copy number, levels of cardiolipin, an inner mitochondrial membrane phospholipid that is critical for proper mitochondrial function, are significantly depleted, a finding further suggesting compromised mitochondrial integrity in the failing SV myocardium.[48] Our systematic analysis of mitochondrial function using high-resolution respirometry corroborates these data and determined that the failing SV heart is typified by impaired OXPHOS, including significant reductions in CI and combined CI and CII OXPHOS, as well as diminished uncoupled electron transport capacity (maximal respiratory capacity). Similar to our findings in the human heart, analysis of neonatal mice with a hypoplastic left ventricle (LV)

FIGURE 6 Continued

(A) Unbiased principal component analysis of single-ventricle nonfailing (SVNF) vs biventricular nonfailing (BVNF) (using significantly dysregulated metabolites) illustrates segregation of each group among the principal components. **(B)** Reactfoam illustration of significantly dysregulated canonical pathways in biventricular nonfailing vs all single-ventricle nonfailing samples identified with Reactome using the differentially expressed metabolites that changed significantly in all single-ventricle nonfailing samples; Fisher's exact test, $-\log_{10}$ (*P* value) >1.3 or $P < 0.05$ (significant pathways **highlighted in yellow**). **(C)** Significantly dysregulated canonical pathways in biventricular nonfailing vs all single-ventricle nonfailing samples identified using integrated pathway and network analysis of both differentially expressed genes (DEGs) and significantly differentially regulated metabolites using MetaboAnalyst. Graphic depicts the pathway impact (x-axis, on the basis of the number of genes or metabolites differentially regulated) and the log odds of a pathway being differentially expressed (y-axis); Fisher's exact test, $-\log_{10}$ (*P* value) >1.3 or $P < 0.05$ **(above dotted line);** relevant significant pathways are identified in boxes. **(D)** Unbiased principal component analysis (PCA) of single-ventricle heart failure vs biventricular nonfailing (using significantly dysregulated metabolites) illustrates segregation of each group among the principal components. **(E)** Reactfoam illustration of significantly dysregulated canonical pathways in biventricular nonfailing vs all single-ventricle heart failure samples identified with Reactome using the 85 differentially expressed metabolites that changed significantly in all single-ventricle heart failure samples; Fisher's exact test, $-\log_{10}$ (*P* value)>1.3 or $P < 0.05$ (significant pathways **highlighted in yellow). (F)** Significantly dysregulated canonical pathways in biventricular nonfailing vs all single-ventricle heart failure samples identified using integrated pathway and network analysis of both differentially expressed genes and significantly differentially regulated metabolites using MetaboAnalyst. Graphic depicts the pathway impact (x-axis, on the basis of the number of genes or metabolites differentially regulated) and the log odds of a pathway being differentially expressed (y-axis); Fisher's exact test, $-\log_{10}$ (*P* value) >1.3 or $P < 0.05$ **(above dotted line);** relevant significant pathways are identified in boxes. ABC = adenosine triphosphate–binding cassette; BCAA = branched-chain amino acid; cGMP = cyclic guanosine monophosphate; DEMs = differentially expressed metabolites; HIPPO = xxx; OXPHOS = oxidative phosphorylation; PC = principal component; PKG = xxx; TCA = tricarboxylic acid; WNT = xxx.

FIGURE 7 **TCA Cycle Flux and Amino Acid Metabolism Are Dysregulated in Subjects**

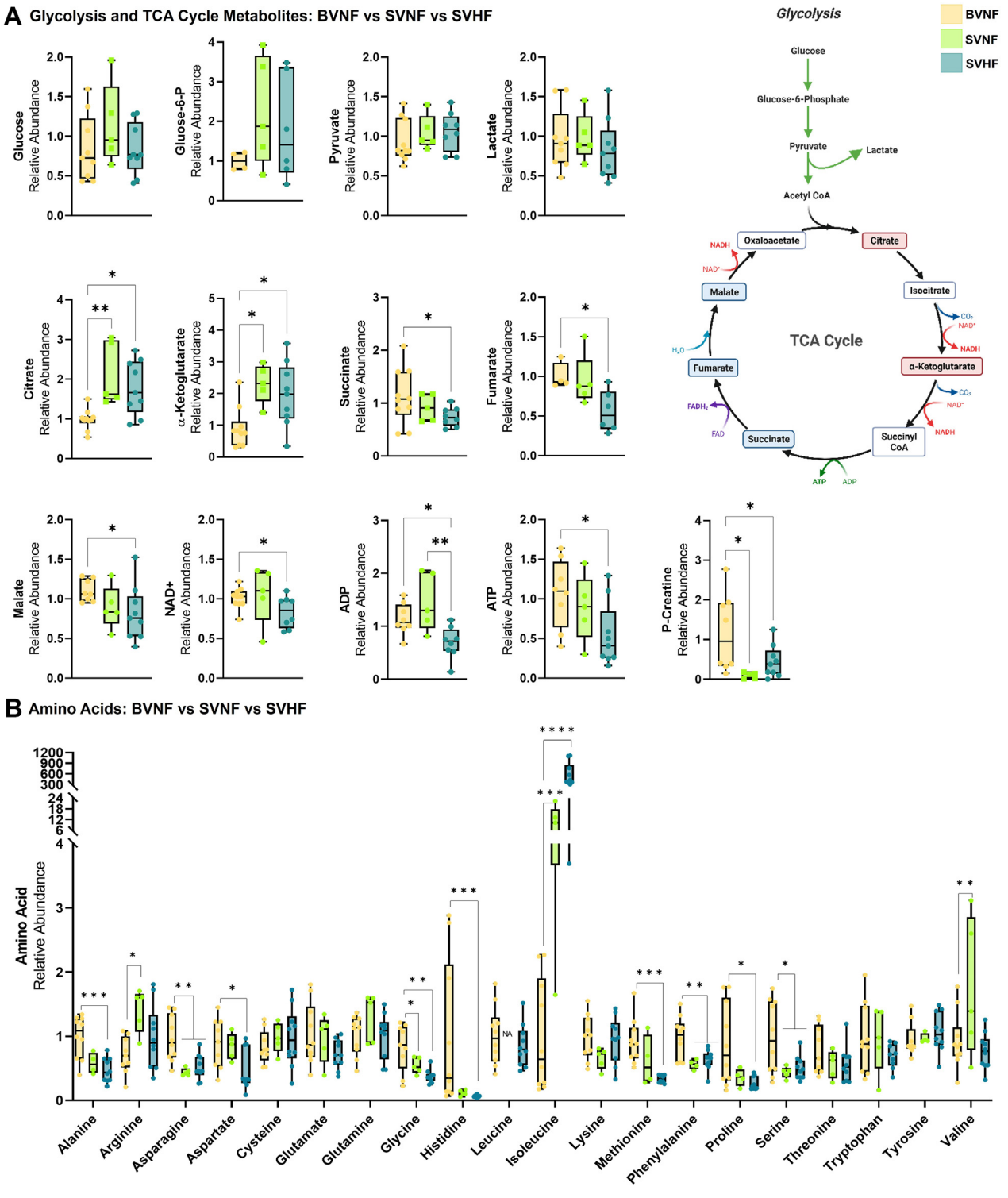

Continued on the next page

and an induced pluripotent stem cell-derived model of HLHS identified alterations in mitochondrial metabolism, thereby suggesting that dysregulated cardiometabolic function may be both a cause and a consequence of SV failure.[60,61] Together, these findings suggest the potential for mitochondrial targeted therapies in this group of patients with few other options.

Both dietary and endogenous AAs contribute to an important common metabolic pool in the body and can be stored, integrated into proteins, or shuttled and catabolized for energy generation. AAs must be properly balanced because they represent important signaling molecules regulating metabolism, protein synthesis, and autophagy.[62] Interestingly, many AAs are significantly decreased in the failing SV myocardium, and possible implications of this phenomenon could include decreased muscle protein synthesis, intracellular signaling, and energetics. Post-Fontan patients with SV have significantly decreased serum concentrations of asparagine, histidine, and threonine, further highlighting the relevance of AA metabolism in the SV heart.[63] Alternatively, elevations in specific AAs, such as BCAAs are associated with numerous systemic diseases, including cancer, diabetes, and HF. The BCAAs leucine, isoleucine, and valine are important modulators of autophagic flux and have a role in mitochondrial quality control.[64-66] However, each of these BCAAs also has distinct biologic effects. Specifically, levels of isoleucine were dramatically increased in the SV heart irrespective of HF, increased levels of isoleucine could mediate alterations in autophagic flux and subsequent accumulation of damaged mitochondria. Additionally, through anaplerotic reactions, AAs can be substantially involved in TCA cycle flux. Elevation of BCAAs and defects in BCAA catabolic activities are emerging as metabolic and molecular contributors to the HF phenotype. However, much of our current knowledge is based on correlative observations in animal models of heart diseases; therefore, it remains unclear whether 1 BCAA or all BCAAs may be necessary and sufficient to promote pathologic myocardial remodeling. Additionally, there is much to be determined with respect to the specific mechanisms by which specific BCAA abundance or regulation may modulate HF progression in different human disease states. Therefore, attaining proper balance of myocardial AAs, some of which can be used as alternative sources of energy, may represent yet another novel therapeutic intervention for SV failure. Future studies are planned to investigate autophagic and mitophagic flux and mitochondrial morphology and integrity as mechanisms of HF progression in the SV heart.

STUDY LIMITATIONS. Although this study represents the most comprehensive multiomic and functional characterization of SV, several limitations deserve consideration. The tissue bank-based aspect of the multiomics analysis in this study is inherently cross-sectional, and as such, determination of whether changes are pathologic or compensatory is not possible. Moreover, studies of SV are challenged by small subject numbers because of the rarity of the condition. We recognize that comparisons of patients with SV at various stages of surgical palliation may exhibit differences in systemic right ventricular volume load that may influence gene expression and metabolic function. Additionally, global metabolomic and transcriptomic studies of human heart tissue, especially in SV CHD, are influenced by multiple factors in addition to palliation stage, including heterogeneity within the myocardium (septum, apex, free wall), genetic diversity among patients, medical comorbidities, duration of HF, degree of cyanosis, gestational age, diet, or the role of specific

FIGURE 7 Continued

(A) Mass spectrometry-based metabolomics analysis of glycolysis and tricarboxylic acid (TCA) cycle intermediates in biventricular nonfailing (BVNF), single-ventricle nonfailing (SVNF), and single-ventricle heart failure (SVHF) myocardial samples. For all groups, box and whisker plot shows mean (bar) and minimum to maximum (ends); each point represents individual patient values (n = 10, biventricular nonfailing; n = 5, single-ventricle nonfailing; and n = 10, single-ventricle heart failure samples); **asterisks** denote significant differences among groups; *P <0.05 and **P <0.01; analysis of variance and Holm-Sidak for citrate, malate, succinate, adenosine diphosphate (ADP), nicotinamide adenine dinucleotide (NAD^+), and phosphocreatine; Kruskal-Wallis test and Dunn's for α-ketoglutarate, fumarate, and adenosine triphosphate (ATP). **(B)** Mass spectrometry-based metabolomics analysis of all amino acids in biventricular nonfailing, single-ventricle nonfailing, and single-ventricle heart failure myocardial samples. For all groups, box and whisker plot shows mean (bar) and minimum to maximum (ends); each point represents individual patient values (n = 10, biventricular nonfailing; n = 5, single-ventricle nonfailing; and n = 10, single-ventricle heart failure samples); **asterisks** denote significant differences among groups; *P <0.05, **P <0.01, ***P <0.001, and ****P <0.0001; analysis of variance and Holm-Sidak for asparagine, phenylalanine, and serine; Kruskal-Wallis test and Dunn's for aspartate, glycine, histidine, isoleucine, methionine, and proline. CoA = coenzyme A; FAD = flavin adenine dinucleotide; FADH = reduced form of flavin adenine dinucleotide; NA = not applicable; NADH = reduced form of nicotinamide adenine dinucleotide; P-creatine = phosphocreatine.

FIGURE 8 **Summary of Impaired Molecular and Bioenergetic Pathways in Single Ventricle**

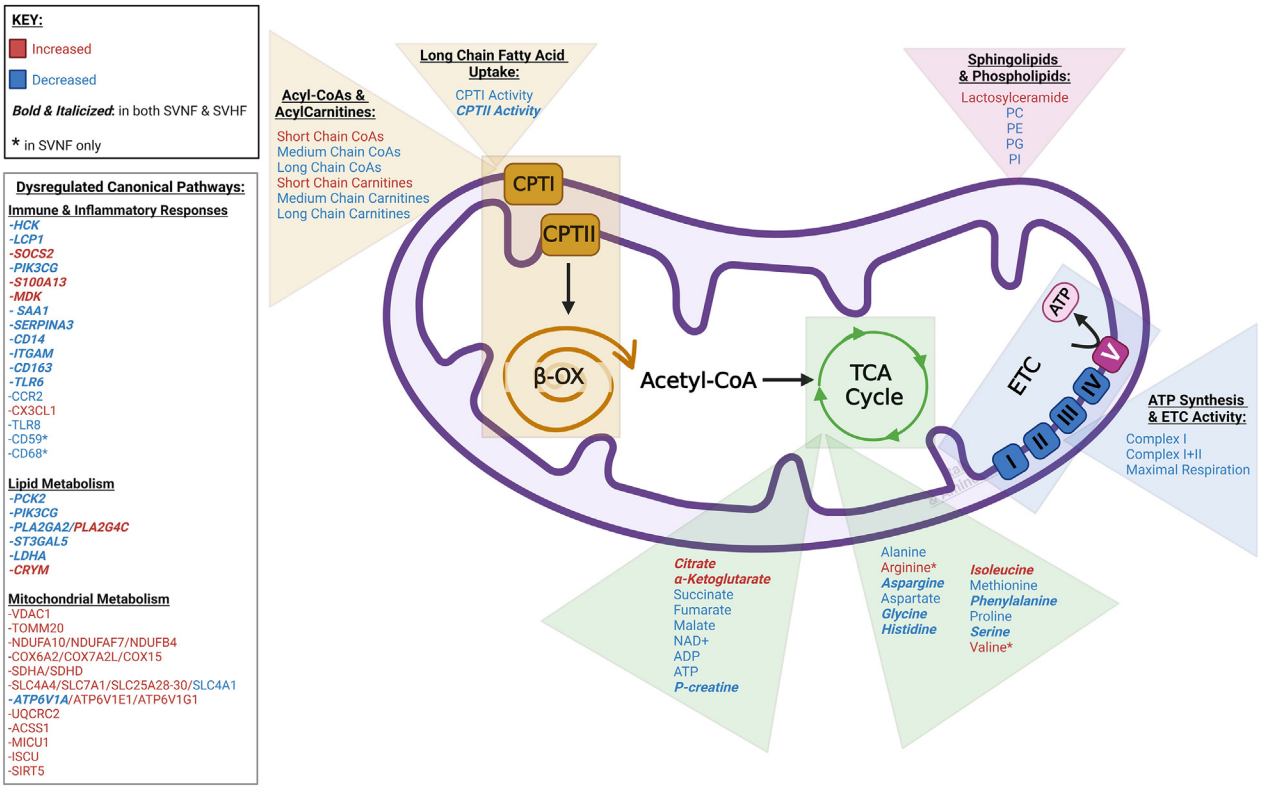

Model of integrated multiomic and functional cardiac bioenergetics analysis in single-ventricle heart disease. **Red text** indicates an increase, whereas **blue text** indicates a decrease relative to biventricular nonfailing (BVNF) control subjects. Normal text indicates the change occurs solely in the single-ventricle heart failure (SVHF) group, an **asterisk** indicates a change solely in the single-ventricle nonfailing (SVNF) group, and text that is both bold and italicized indicates a change in both single-ventricle nonfailing and single-ventricle heart failure groups. CPT = carnitine palmitoyltransferase; ETC = electron transport chain; β-OX, β-oxidation; PC = phosphatidylcholine; PE = phosphatidylethanolamine; PG = phosphatidylglycerol; PI = phosphatidylinositol; other abbreviations as in **Figure 7**. Created with BioRender.com.

medications. Additionally, because it is uncommon for a pediatric donor heart to go unmatched, it is difficult to attain age-matched control heart tissue. For some pediatric BVNF samples, limited demographics data are available. We also recognize that our SVNF samples are inherently from younger patients than our SVHF and BVNF samples because these patients undergo the Norwood-Sano procedure or primary cardiac transplantation in the first few weeks to months of life. However, despite these age differences, metabolic gene expression and some lipid and metabolite species in these patients are similar to those seen in BVNF control subjects and do not correlate with age. This finding suggests that age is not the primary variable accounting for our detected changes among groups. Our experiments were performed using explanted myocardium, and we acknowledge that the data are not representative of cardiomyocytes alone, and relative contributions of the extracellular matrix, fibroblasts, endothelial cells, immune cells, or other cell types therefore cannot be determined. Because pediatric explanted heart tissue is an extremely limited resource, we chose to perform this initial transcriptomics analysis using bulk RNA-Seq. Future studies are planned to perform single-nuclei RNA-Seq to refine our understanding of the

molecular dynamics of various cell types in the SV heart further. Additionally, we recognize that tissue-level metabolic measurements do not provide definitive conclusions on alterations in myocardial metabolic flux and substrate use. Finally, we included only SV subjects with a single RV, and we subsequently elected to use RV tissue, as opposed to LV tissue, from our BVNF subjects to eliminate the influence of underlying ventricular morphology. Although RV vs LV comparisons may be interesting, the normal postnatal RV maintains a cardiac output equal to that of the LV at approximately one-fifth of the energy cost, and even though right ventricular metabolism and right ventricular metabolism have shared characteristics, they also have several unique properties.[67,68] Therefore, the innate metabolic differences between the LV and the RV would limit the interpretation of comparisons between the systemic RV and the normal or failing LV. Nevertheless, this study addresses important gaps in knowledge, by providing novel and valuable insight into the molecular pathways and functional changes in the SV heart that deserve further study given the absence of evidence-based therapies to prevent or treat HF in this growing group of patients.

CONCLUSIONS

Unbiased integrated multiomics investigations together with functional bioenergetics analysis suggest that the SV heart is characterized by transcriptomic remodeling and impaired cardiac bioenergetics to varying degrees depending on the presence of HF. The failing SV heart displays decreased metabolic intermediates, diminished mitochondrial CPTI and CPTII enzyme activity, reduced mitochondrial OXPHOS, and impaired cardiac energy generation. These data further support our hypothesis that the failing SV heart is energy starved, primarily in response to a decreased availability of reducing equivalents, an altered lipid milieu, diminished long-chain FA uptake by the mitochondria, and impaired mitochondrial respiratory chain function. Interestingly, although altered cardiometabolic function may be a final common pathway of HF regardless of origin, some of these bioenergetic perturbations precede the onset of overt failure and are seen in nonfailing SV myocardium, findings suggesting vulnerability of the normally functioning SV heart. Therefore, these results provide novel information on some of the mechanisms involved in the transition to HF in patients with SV CHD, and they contribute to the identification of promising novel therapeutic targets aimed at the treatment or prevention of SV failure in a group of patients with few other options.

ACKNOWLEDGMENTS The authors are deeply appreciative of all patients with SV, and their parents, seen at Children's Hospital Colorado for their agreement to participate in this study. The authors would like to acknowledge the Heart Transplant Team at Children's Hospital Colorado, especially Drs David Campbell, Max Mitchell, James Jaggers, and Matthew Stone for their assistance with obtaining explanted heart tissue; and Sam Schofield, Alix Michael, Jacqueline Holstein, Megyn Gordon, and Meghan Williams for data collection and subject recruitment. The authors also acknowledge the Pediatric Cardiovascular Research Laboratory on-call team at the University of Colorado Anschutz Medical Campus for the rapid dissection and transportation of fresh cardiac specimens to the laboratory.

FUNDING SUPPORT AND AUTHOR DISCLOSURES

This work was supported by the National Institutes of Health National Heart Lung and Blood Institute (R01 HL126928[SDM, CCS, BLS], R01 HL126928-03S1[AMG]), the National Center for Advancing Translational Sciences Colorado Clinical and Translational Sciences Institute awards (UL1-TR002535, KL2-TR002534, and TL1-TR002533), the Addison Scott Memorial Fund, the Boedecker Foundation, the Nair Family, the Rose Community Foundation, and the Jack Cooper Millisor Chair in Pediatric Heart Disease. Dr. Sucharov has served as a scientific founder at miRagen, Inc. All other authors have reported that they have no relationships relevant to the content of this paper to disclose.

ADDRESS FOR CORRESPONDENCE: Dr Shelley Miyamoto, Division of Cardiology, Department of Pediatrics, University of Colorado Anschutz Medical Campus, Children's Hospital Colorado, 13123 East 16th Ave, B100, Aurora, Colorado 80045, USA. E-mail: shelley.miyamoto@childrenscolorado.org. Twitter: @ShelleyMiyamoto. OR Dr Carmen C. Sucharov, Division of Cardiology, Department of Medicine, University of Colorado Anschutz Medical Campus, 12700 East 19th Avenue, B139, Aurora, Colorado 80045, USA. E-mail: kika.sucharov@cuanschutz.edu.

PERSPECTIVES

COMPETENCY IN MEDICAL KNOWLEDGE: The *failing* SV heart is typified by alterations in metabolic gene expression associated with diminished ATP and phosphocreatine levels, decreased activity of CPT transporters, and impaired OXPHOS and maximal respiratory capacity. The *nonfailing* SV heart demonstrates an intermediate metabolic phenotype suggesting that the SV heart is vulnerable to eventual failure; these results provide some insights into the transition from health to disease in SV CHD.

TRANSLATIONAL OUTLOOK: This study presents a comprehensive characterization of the transcriptome combined with functional mitochondrial studies in SV CHD myocardium. Results from this study suggest that mitochondrial targeted therapies, including treatments aimed at preserving or restoring the potential to generate energy, in the SV heart could have the potential to prevent or treat SV HF.

REFERENCES

1. Miranović V. The incidence of congenital heart disease: previous findings and perspectives. *Srp Arh Celok Lek*. 2014;142:243-248.

2. Julsrud PR, Weigel TJ, Van Son JA, et al. Influence of ventricular morphology on outcome after the Fontan procedure. *Am J Cardiol*. 2000;86:319-323.

3. McGuirk SP, Winlaw DS, Langley SM, et al. The impact of ventricular morphology on midterm outcome following completion total cavopulmonary connection. *Eur J Cardiothorac Surg*. 2003;24:37-46.

4. Anderson PA, Sleeper LA, Mahony L, et al. Contemporary outcomes after the Fontan procedure: a Pediatric Heart Network multicenter study. *J Am Coll Cardiol*. 2008;52:85-98.

5. Alsoufi B, Manlhiot C, Awan A, et al. Current outcomes of the Glenn bidirectional cavopulmonary: connection for single ventricle palliation. *Eur J Cardiothorac Surg*. 2012;42:42-49.

6. Backer CL. The functionally univentricular heart: which is better-right or left ventricle? *J Am Coll Cardiol*. 2012;59:1186-1187.

7. D'Udekem Y, Xu MY, Galati JC, et al. Predictors of survival after single-ventricle palliation: the impact of right ventricular dominance. *J Am Coll Cardiol*. 2012;59:1178-1185.

8. Lotto AA, Hosein R, Jones TJ, Barron DJ, Brawn WJ. Outcome of the Norwood procedure in the setting of transposition of the great arteries and functional single left ventricle. *Eur J Cardiothorac Surg*. 2009;35:149-155.

9. Kogon BE, Plattner C, Leong T, Simsic J, Kirshbom PM, Kanter KR. The bidirectional Glenn operation: a risk factor analysis for morbidity and mortality. *J Thorac Cardiovasc Surg*. 2008;136:1237-1242.

10. Daebritz SH, Nollert GDA, Zurakowski D, et al. Results of Norwood stage I operation: comparison of hypoplastic left heart syndrome with other malformations. *J Thorac Cardiovasc Surg*. 2000;119:358-367.

11. Alsoufi B, Gillespie S, Kim D, et al. The impact of dominant ventricle morphology on palliation outcomes of single ventricle anomalies. *Ann Thorac Surg*. 2016;102:593-601.

12. Coats L, O'Connor S, Wren C, O'Sullivan J. The single-ventricle patient population: a current and future concern a population-based study in the north of England. *Heart*. 2014;100:1348-1353.

13. Shaddy RE, Boucek MM, Hsu DT, et al. Carvedilol for children and adolescents with heart failure: a randomized controlled trial. *JAMA*. 2007;298:1171-1179.

14. Hsu DT, Zak V, Mahony L, et al. Enalapril in infants with single ventricle: results of a multicenter randomized trial. *Circulation*. 2010;122:333-340.

15. Oldenburger NJ, Mank A, Etnel J, Takkenberg JJM, Helbing WA. Drug therapy in the prevention of failure of the Fontan circulation: a systematic review. *Cardiol Young*. 2016;26:842-850.

16. Dzau V. Clinical implications for therapy: possible cardioprotective effects of ACE inhibition. *Br J Clin Pharmacol*. 1989;28(suppl 2):183S-187S.

17. Menon SC, Erickson LK, McFadden M, Miller DV. Effect of ventriculotomy on right-ventricular remodeling in hypoplastic left heart syndrome: a histopathological and echocardiography correlation study. *Pediatr Cardiol*. 2013;34:354-363.

18. Ohye RG, Schonbeck JV, Eghtesady P, et al. Cause, timing, and location of death in the Single Ventricle Reconstruction trial. *J Thorac Cardiovasc Surg*. 2012;144:907-914.

19. Khairy P, Fernandes SM, Mayer JE, et al. Long-term survival, modes of death, and predictors of mortality in patients with Fontan surgery. *Circulation*. 2008;117:85-92.

20. Wu TD, Nacu S. Fast and SNP-tolerant detection of complex variants and splicing in short reads. *Bioinformatics*. 2010;26:873-881.

21. Anders S, Pyl PT, Huber W. HTSeq-a Python framework to work with high-throughput sequencing data. *Bioinformatics*. 2015;31:166-169.

22. Robinson MD, McCarthy DJ, Smyth GK. edgeR: a bioconductor package for differential expression analysis of digital gene expression data. *Bioinformatics*. 2009;26:139-140.

23. Ashburner M, Ball CA, Blake JA, et al. Gene ontology: tool for the unification of biology. *Nat Genet*. 2000;25:25-29.

24. Krämer A, Green J, Pollard J, Tugendreich S. Causal analysis approaches in Ingenuity Pathway Analysis. *Bioinformatics*. 2014;30:523-530.

25. Zhou Y, Zhou B, Pache L, et al. Metascape provides a biologist-oriented resource for the analysis of systems-level datasets. *Nat Commun*. 2019;10:1523.

26. Piñero J, Queralt-Rosinach N, Bravo À, et al. DisGeNET: a discovery platform for the dynamical exploration of human diseases and their genes. *Database (Oxford)*. 2015;2015:bav028.

27. Piñero J, Bravo Á, Queralt-Rosinach N, et al. DisGeNET: A comprehensive platform integrating information on human disease-associated genes and variants. *Nucleic Acids Res*. 2017;45:D833-D839.

28. Mi H, Muruganujan A, Casagrande JT, Thomas PD. Large-scale gene function analysis with the PANTHER classification system. *Nat Protoc*. 2013;8:1551-1566.

29. Mi H, Muruganujan A, Ebert D, Huang X, Thomas PD. PANTHER version 14: more genomes, a new PANTHER GO-slim and improvements in enrichment analysis tools. *Nucleic Acids Res*. 2018;47:419-426.

30. Mi H, Muruganujan A, Huang X, et al. Protocol update for large-scale genome and gene function analysis with the PANTHER classification system (v.14.0). *Nat Protoc*. 2019;14:703-721.

31. Thomas PD, Campbell MJ, Kejariwal A, et al. PANTHER: a library of protein families and subfamilies indexed by function. *Genome Res*. 2003;13:2129-2141.

32. Clasquin MF, Melamud E, Rabinowitz JD. LC-MS data processing with MAVEN: a metabolomic analysis and visualization engine. *Curr Protoc Bioinformatics*. 2012 Chapter 14:Unit14.11.

33. Vastrik I, D'Eustachio P, Schmidt E, et al. Reactome: a knowledge base of biologic pathways and processes. *Genome Biol*. 2007;8:R39.

34. Fabregat A, Sidiropoulos K, Viteri G, et al. Reactome pathway analysis: a high-performance in-memory approach. *BMC Bioinformatics*. 2017;18:142.

35. Sidiropoulos K, Viteri G, Sevilla C, et al. Reactome enhanced pathway visualization. *Bioinformatics*. 2017;33:3461-3467.

36. Fabregat A, Korninger F, Viteri G, et al. Reactome graph database: efficient access to complex pathway data. *PLoS Comput Biol*. 2018;14:e1005968.

37. Jassal B, Matthews L, Viteri G, et al. The reactome pathway knowledgebase. *Nucleic Acids Res*. 2020;48:D649-D655.

38. Xia J, Psychogios N, Young N, Wishart DS. MetaboAnalyst: a web server for metabolomic data analysis and interpretation. *Nucleic Acids Res*. 2009;37:W652-W660.

39. Chong J, Soufan O, Li C, et al. MetaboAnalyst 4.0: towards more transparent and integrative metabolomics analysis. *Nucleic Acids Res*. 2018;46:W486-W494.

40. Chong J, Xia J, MetaboAnalystR. An R package for flexible and reproducible analysis of metabolomics data. *Bioinformatics*. 2018;34:4313-4314.

41. Yoon HR, Hong YM, Boriack RL, Bennett MJ. Effect of L-carnitine supplementation on cardiac carnitine palmitoyltransferase activities and plasma carnitine concentrations in adriamycin-treated rats. *Pediatr Res*. 2003;53:788-792.

42. Chatfield KC, Sparagna GC, Chau S, et al. Elamipretide improves mitochondrial function in the failing human heart. *J Am Coll Cardiol Basic Trans Science*. 2019;4:147-157.

43. Palladino AA, Chen J, Kallish S, Stanley CA, Bennett MJ. Measurement of tissue acyl-CoAs using flow-injection tandem mass spectrometry: acyl-CoA profiles in short-chain fatty acid oxidation defects. *Mol Genet Metab*. 2012;107:679-683.

44. Bielawski J, Pierce JS, Snider J, Rembiesa B, Szulc ZM, Bielawska A. Comprehensive quantitative analysis of bioactive sphingolipids by high-performance liquid chromatography-tandem mass spectrometry. *Methods Mol Biol*. 2009;579:443-467.

45. Harrison KA, Bergman BC. HPLC-MS/MS methods for diacylglycerol and sphingolipid molecular species in skeletal muscle. *Methods Mol Biol*. 2019;1978:137-152.

46. Sparagna GC, Johnson CA, McCune SA, Moore RL, Murphy RC. Quantitation of cardiolipin molecular species in spontaneously hypertensive heart failure rats using electrospray ionization mass spectrometry. *J Lipid Res*. 2005;46:1196-1204.

47. Bligh EG, Dyer WJ. A rapid method of total lipid extraction and purification. *Can J Biochem Physiol*. 1959;37:911-917.

48. Garcia AM, McPhaul JC, Sparagna GC, et al. Alteration of cardiolipin biosynthesis and remodeling in single right ventricle congenital heart disease. *Am J Physiol Heart Circ Physiol*. 2020;318:H787-H800.

49. Sparagna GC, Chicco AJ, Murphy RC, et al. Loss of cardiac tetralinoleoyl cardiolipin in human and experimental heart failure. *J Lipid Res*. 2007;48:1559-1570.

50. Piñero J, Ramírez-Anguita JM, Saüch-Pitarch J, et al. The DisGeNET knowledge platform for disease genomics: 2019 update. *Nucleic Acids Res*. 2020;48:D845-D855.

51. Brown DA, Perry JB, Allen ME, et al. Mitochondrial function as a therapeutic target in heart failure. *Nat Rev Cardiol*. 2017;14:238-250.

52. Deya-Martinez A, Flinn AM, Gennery AR. Neonatal thymectomy in children—accelerating the immunologic clock? *J Allergy Clin Immunol*. 2020;146:236-243.

53. Kurobe H, Tominaga T, Sugano M, et al. Complete but not partial thymectomy in early infancy reduces T-cell-mediated immune response: three-year tracing study after pediatric cardiac surgery. *J Thorac Cardiovasc Surg*. 2013;145:656-662.e2.

54. Appachi E, Mossad E, Mee RBB, Bokesch P. Perioperative serum interleukins in neonates with hypoplastic left-heart syndrome and transposition of the great arteries. *J Cardiothorac Vasc Anesth*. 2007;21:184-190.

55. Jain PN, Robertson M, Lasa JJ, et al. Altered metabolic and inflammatory transcriptomics after cardiac surgery in neonates with congenital heart disease. *Sci Rep*. 2021;111:4965.

56. Murashige D, Jang C, Neinast M, et al. Comprehensive quantification of fuel use by the failing and nonfailing human heart. *Science*. 2020;370:364.

57. Schönfeld P, Wojtczak L. Short- and medium-chain fatty acids in energy metabolism: the cellular perspective. *J Lipid Res*. 2016;57:943-954.

58. Russell L, Finck B, Kelly D. Mouse models of mitochondrial dysfunction and heart failure. *J Mol Cell Cardiol*. 2005;38:81-91.

59. Paridon SM, Mitchell PD, Colan SD, et al. A cross-sectional study of exercise performance during the first 2 decades of life after the Fontan operation. *J Am Coll Cardiol*. 2008;52:99-107.

60. Liu X, Yagi H, Saeed S, et al. The complex genetics of hypoplastic left heart syndrome. *Nat Genet*. 2017;49:1152-1159.

61. Xu X, Jin K, Bais AS, et al. Uncompensated mitochondrial oxidative stress underlies heart failure in an iPSC-derived model of congenital heart disease. *Cell Stem Cell*. 2022;29:840-855.e7.

62. Nesterov SV, Yaguzhinsky LS, Podoprigora GI, Nartsissov YR. Amino acids as regulators of cell metabolism. *Biochemistry (Mosc)*. 2020:393-408.

63. Michel M, Dubowy KO, Entenmann A, et al. Targeted metabolomic analysis of serum amino acids in the adult Fontan patient with a dominant left ventricle. *Sci Rep*. 2020;10:8930.

64. Sun H, Olson KC, Gao C, et al. Catabolic defect of branched-chain amino acids promotes heart failure. *Circulation*. 2016;133:2038-2049.

65. De Pasquale V, Caterino M, Costanzo M, Fedele R, Ruoppolo M, Pavone LM. Targeted metabolomic analysis of a mucopolysaccharidosis IIIB mouse model reveals an imbalance of branched-chain amino acid and fatty acid metabolism. *Int J Mol Sci*. 2020;21:1-21.

66. Li T, Zhang Z, Kolwicz SC, et al. Defective branched-chain amino acid catabolism disrupts glucose metabolism and sensitizes the heart to ischemia-reperfusion injury. *Cell Metab*. 2017;25:374-385.

67. Heiskanen MA, Leskinen T, Eskelinen JJ, et al. different predictors of right and left ventricular metabolism in healthy middle-aged men. *Front Physiol*. 2015;6:389.

68. Friedberg MK, Redington AN. Right versus left ventricular failure: differences, similarities, and interactions. *Circulation*. 2014;129:1033-1044.

KEY WORDS cardiac metabolism, cardiometabolic remodeling, heart failure, hypoplastic left heart syndrome, mitochondria, oxidative phosphorylation, single ventricle

APPENDIX For supplemental tables and figures, please see the online version of this paper.